(E76-10217) USE OF SKYLAB EREP DATA IN A SEA-SURFACE TEMPERATURE EXPERIMENT Final Report, 17 Feb. 1973 - 1 Aug. 1975 (JRB Associates, Ann Arbor, Mich.) 54 p HC $4.50 CSCL 08J G3/43

N76-19520

Unclas
00217

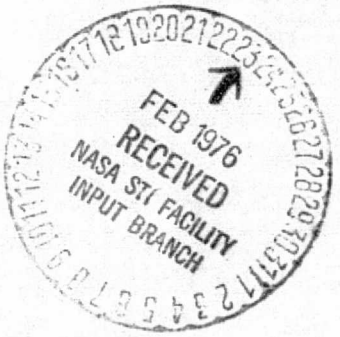

jb associates

JRB-75-202-AA

USE OF SKYLAB EREP DATA IN A SEA-SURFACE TEMPERATURE EXPERIMENT

Final Report

David C. Anding
John P. Walker

Science Applications, Incorporated
Ann Arbor, Michigan 48103

Prepared for

National Aeronautics and Space Administration
Johnson Space Center
Houston, Texas 77058

Contract NAS9-13277

July 1975

JRB ASSOCIATES
15 Research Drive, P. O. Box 328, Ann Arbor, MI 48103, (313)662-3261

FOREWORD

The research described herein, which was conducted by JRB Associates - a wholly owned subsidiary of Science Applications, Incorporated, was performed under NASA Contract NAS9-13277. This final report under the contract covers the period 17 February 1973 to 1 August 1975.

ABSTRACT

This final report discusses the utilization of Skylab EREP data in a sea surface temperature experiment demonstrating the feasibility of a procedure for the remote measurement of sea-surface temperature which inherently corrects for the effect of the intervening atmosphere without recourse to climatological data. The procedure relies upon the near-linear differential absorption properties of the infrared window region between 10 and 13 μm and requires radiometric measurements in a minimum of two spectral intervals within the infrared window which have a significant difference in absorption coefficient. The procedure has been applied to Skylab EREP S191 spectrometer data and it is demonstrated that atmospheric effects on the observed brightness temperature can be reduced to less than 1.0° K.

TABLE OF CONTENTS

FIGURES

FIGURES (Continued)

USE OF SKYLAB EREP DATA IN A SEA-SURFACE TEMPERATURE EXPERIMENT

SUMMARY

Accurately mapping the sea-surface temperature from remote radiometric measurements requires accurate compensation of the effects of the intervening atmosphere on the observed radiance. These effects can decrease the observed radiometric temperature of the sea surface by as much as 8^{o} K, depending upon the atmospheric temperature and humidity, and the altitude and nadir angle of observation. Operational sensors aboard NOAA satellites measure the radiance in a spectral band extending from 10.5 to 12.5 μm at a ground spatial resolution of approximately 0.5 nautical miles. The effects of the intervening atmosphere on the observed radiance values are compensated by applying radiative transfer models to prevailing values of atmospheric temperature and humidity which are estimated from climatological data or obtained from soundings. The correctness of the result depends upon the accuracy of the radiative transfer models and the precision to which the atmospheric data are known. This report discusses a procedure for estimating sea-surface temperature from radiometric data without recourse to climatological data. The method relies on differential extinction in the 10 - 13 μm spectral region from which the amount of atmospheric extinction and emission can be inferred. The differential extinction is approximately linear so application of the method requires measurements in at least two radiometric bands between 10 and 13 μm.

The success of the procedure results from a near linear relationship between atmospheric absorption and atmospheric extinction coefficient in the spectral region from 10 to 13 μm, and a monotonic

increase in the average extinction coefficient as the wavelength is increased from 10 μm. This report presents the mathematical foundation of the procedure and demonstrates its plausibility with synthesized multiband radiometric data. Actual procedural results are demonstrated through the use of Nimbus-4 IRIS data and EREP S191 infrared spectrometer data.

The EREP experiment consisted of acquiring spectrometer data (~6 to ~15 μm) over ocean areas for which the atmospheric temperature and humidity, and sea-surface temperature were known. The air and surface truth data were input to radiative transfer models and the spectral radiance one would expect at the entrance aperture of the S191 spectrometer was calculated. These results were compared with EREP S191 data in the 10 to 13 μm spectral region and the validity of the radiative transfer models (within EREP experimental accuracy) are demonstrated. Also, for two EREP test sites (Key West and the Monroe Reservoir) the sea-surface temperature was estimated from EREP data and the results compared with surface truth.

The next generation of TIROS satellites will contain two channels in the infrared window region for purposes of more accurate measurement of sea-surface temperature. The initial design of the instrument has been finalized (including signal-to-noise and absolute calibration requirements) but the spectral response of each of the two channels remains open. It is felt that the results of the analysis presented herein should have an impact on the selection of the two radiometric channels.

1
INTRODUCTION

Global measurement of sea-surface temperature (hereafter referred to as SST) on a daily basis is currently operational at NOAA's National Environmental Satellite Service (NESS) Center. SST data are archived after a rather complex analysis of data from the scanning radiometer (SR) aboard the NOAA-4 satellite. The procedure for extracting SST information from SR data is an extension of that of Smith and Rao [1]. Basically, infrared window measurements (10.5 - 12.5 μm) are converted to SST values, at degraded spatial resolution, with proper consideration of SR instrument noise, noise related to signal transmission, receiving and processing, and after accounting for the effects of the intervening atmosphere based upon climatological data.

Because of inherent limitations in the single-channel scanning radiometer method of producing SST's, archived temperatures have limited accuracy and spatial resolution. The next generation of TIROS satellites, denoted TIROS-N series, will contain a five-channel advanc ery high resolution radiometer (AVHRR), which will provide for improved SST retrieval. The first instrument to be flown, planned for FY 78, will contain four channels, with a fifth channel to be added on the fourth or fifth satellite in the TIROS-N series. The nominal spectral regions for each of the five channels are 0.55 to 0.9 μm, 0.72 μm to detector cutoff (approximately 1.0 μm), 3.55 to 3.93 μm, 10.5 to 11.5 μm, and 11.5 to 12.5 μm, which will be the fifth channel to be added. The spectral response of the first four channels has been finalized, however, the spectral response of the fifth channel is still open. Of major impact to SST measurement is the addition of the infrared channel from 3.55 - 3.93 μm and the division of the present infrared window channel, i.e., 10.5 - 12.5 μm, into two channels. The reason for the addition of the two

infrared channels is to provide additional information to correct for the effects of atmospheric moisture on the observed radiance, which can be significant, particularly for warm and moist conditions, without recourse to climatological data.

Previous studies [2, 3, 4, 5] have indicated that the addition of a second channel in the infrared window, one somewhat less transparent than the other, would allow for compensation of the effects of absorption and emission by atmospheric water vapor without recourse to climatological or other supportive data. The investigations involved the use of radiative transfer models, and large field-of-view space acquired data, i. e., the infrared interferometer (IRIS) aboard Nimbus 4. Although the results were encouraging, they remained tentative until they could be verified by an experiment for which the sensor field-of-view was comparable to that which will be used on future TIROS satellites. The Skylab mission provided the first opportunity for such a verification experiment.

The planned Skylab experiment was to acquire long-wavelength S191 spectrometer data over several ocean areas for which the SST and atmospheric conditions were known. The objective was to utilize these data in validating the radiative transfer models used in the initial investigations, and to test the validity and correctness of two-channel temperature estimating algorithms developed from the radiative transfer models. A further purpose of the experiment was to acquire long wavelength S191 data for cloud filled fields of view for comparison with radiative transfer model computations.

During the period between planning the experiment and the actual acquisition and analysis of data, significant advances in the state-of-knowledge of atmospheric absorption and emission occurred. A consequence of these advancements was the realization that the radiative

transfer models used for the initial investigations were somewhat inaccurate. Furthermore, because the two-channel SST estimating algorithms were derived from the radiative transfer models, they also were inaccurate. As part of the Skylab investigation it was therefore necessary to revise the radiative transfer models and redefine the temperature estimating algorithms.

S191 data were acquired for ten test sites and planned for analysis. Although all data were acquired, processed, and analyzed, because of instrument problems the data from only two missions were useful in satisfying the objectives of the experiment. This loss of data was partially offset by the utilization of IRIS data for six locations, the only other source of space acquired long-wavelength spectral data over ocean areas.

The results of the investigation indicated that a significant benefit will be derived by the addition of a second channel in the infrared window region. Specifically, without recourse to climatological data, the investigation indicated SST's could be estimated to within 1^{o} K*. Although the spectral bands selected for the analysis yielded a satisfactory result, the investigation also indicated that the infrared window transmission function contains nonlinearities and uncertain aerosol effects which could have a significant impact upon the optimum choice of the two spectral channels. Based upon the analysis presented herein, the two spectral bands which yielded the best result were 10.25 - 11.25 and 12.0 - 12.9 μm. However, since the present analysis was limited in scope, it is recommended that a further analysis be performed before a final choice of spectral channels is made.

Since the processing and analysis of data from each test site was identical, the only data presented herein are those for the two usable

---

* Temperature accuracies are based upon atmospheric effects only. Other sources of noise and accuracy degradation factors are not included.

Skylab missions and those from IRIS. The data from other missions and the justification for their exclusion is given in earlier progress reports [6, 7, 8, 9].

This final report is divided into three major sections. The first deals with the theoretical basis of remote SST measurements at thermal infrared wavelengths. The second discusses the required modifications to the radiative transfer models and the two-channel temperature estimating algorithm. The final section presents and analyzes the data and discusses the primary results of the investigation.

2

THEORETICAL BASIS OF REMOTE SST MEASUREMENT AT THERMAL INFRARED WAVELENGTHS

The spectral radiance emitted by an opaque body at wavelength λ is given by

$$L(\lambda, T) = \epsilon(\lambda) L^{bb}(\lambda, T), \tag{1}$$

where $\epsilon(\lambda)$ is the spectral emittance of the opaque body and $L^{bb}(\lambda, T)$ is the spectral radiance emitted by a blackbody. The latter is represented as

$$L^{bb}(\lambda, T) = \frac{2hc^2}{\lambda^5 (e^{hc/\lambda kT} - 1)}, \tag{2}$$

where

T = the temperature of a blackbody

c = the velocity of light

h = Planck's constant

λ = wavelength

k = Boltzmann's constant.

It is clear from these expressions that if the emittance is known, the temperature can be determined by measuring the emitted spectral radiance and inverting Eq. (1). The application of such a measurement procedure to determine the temperature of a water surface exposed to the atmosphere is more complex. The spectral emittance of a sea surface is less than unity, the amount depending upon the exittance angle. Consequently, as one attempts to measure the emitted radiation, some sky radiation will be reflected from the water surface and collected by the infrared sensor. Also, since water does not become opaque to infrared radiation at thermal wavelengths until a depth of approximately 0.10 mm, some of the measured radiation emanates from below the surface, which generally has a slightly different temperature. Therefore, the temperature derived from a measurement of the radiance at the surface will be the temperature of a blackbody which yields an equivalent value of radiance (i. e., the "equivalent radiometric temperature"). It will be different from the actual surface temperature; the degree of difference will depend upon the magnitude of the reflected radiation and the temperature gradient near the surface.

The present analysis is not concerned with the relationship between the equivalent radiometric temperature and the actual surface temperature, but only with the effect of the atmosphere on the equivalent radiometric temperature derived from a radiometric measurement performed at satellite altitudes. Therefore, all future references to SST will refer to the equivalent radiometric temperature that would be derived from a radiance measurement at the surface.

Before reaching a spaceborne sensor, the spectral radiance emanating from the sea surface will be attenuated by atmospheric constituents, such as clouds, haze, and absorbing gases. These atmospheric constituents also emit and scatter radiant energy, which contributes to the total signal received by the sensor. The central problem in accurately

measuring SST from space lies in determining the extent to which such effects can be observed and compensated.

To demonstrate more clearly the nature of the problem of measuring the sea temperature from space, consider the spectral radiance leaving the top of the atmosphere, $L(\lambda)$, which can be represented by

$$L(\lambda) = L^{bb}[\lambda, T(P_o)]\tau(\lambda, P_o)\epsilon(\lambda) + \int_{\tau(\lambda, P_o)}^{1} L^{bb}[\lambda, T(P)]\, d\tau(\lambda, P), \qquad (3)$$

where

P_o is surface pressure
τ is atmospheric transmittance
P is atmospheric pressure
T is temperature.

According to Eq. (3) estimating $T(P_o)$ from $L(\lambda)$ requires values of temperature, pressure, and the differential absorption properties of the atmosphere. Estimating SST from a single channel radiometric measurement is analogous to inverting Eq. (3) given temperature and pressure values consistent with the prevailing conditions which are obtained from either atmospheric soundings or climatological data.

To eliminate the requirement for ancillary data a scheme was devised which utilizes more than one spectral channel. The scheme was originally discussed and presented by Anding and Kauth [2], and subsequently discussed by McMillin [3] and Prabhakara [4]. The technique, like most remote sounding methods, is based on the use of the differential optical properties of the atmosphere in the infrared window region to infer the atmospheric attenuation. The attenuation values are then used to correct for the effect of the atmosphere on radiometric data.

Following the development of Prabhakara [4] the radiative transfer equation may be simplified as

$$L(\lambda) = L^{bb}[\lambda, T(P_o)]\tau(\lambda, P_o)\epsilon(\lambda) + \overline{L^{bb}(\lambda)}\,[1 - \tau(\lambda, P_o)], \tag{4}$$

where $\overline{L^{bb}(\lambda)}$ is the weighted mean Planck emission of the atmosphere.

In the infrared window region there are three primary contributors to extinction. Local water vapor Lines, H_2O continuum, and aerosols. The transmission functions for continuum absorption* and aerosols are accurately represented by Beers Law. This is also true for selective line absorption when the absorption is either weak or the individual lines are heavily overlapped. These conditions are approximately satisfied in the window region for one airmass. Hence, window transmission can be expressed as

$$\tau = e^{-(k_\ell + k_c + k_a)u} = e^{-k_t u}, \quad k_t = k_\ell + k_c + k_a \tag{5}$$

where k_ℓ, k_c, k_a and k_t are wavelength dependent and denote the local line, H_2O continuum, aerosol extinction, and total extinction coefficient, respectively. u is the effective absorber thickness. To a good approximation Eq. (5) can be represented by the first two terms of its series expansion, i.e.,

$$\tau \simeq 1 - k_t u. \tag{6}$$

Substituting (6) into (4), and letting $\epsilon(\lambda) = 1$, we have**

$$L(\lambda) \simeq L^{bb}[\lambda, T(P_o)] - \left\{ L^{bb}[\lambda, T(P_o)] - \overline{L^{bb}(\lambda)} \right\} k(\lambda)\, u. \tag{7}$$

---

* In the 10-13 μm region molecules only absorb radiation, but aerosols absorb and scatter radiation. Therefore, the use of the word absorption for molecular effects is correct, and the use of the word extinction is required only for aerosol effects or the effects of the total atmosphere.

** For convenience the subscript t will be dropped and all future values of $k(\lambda)$ denote the total extinction coefficient.

Expanding the Planck function about the surface temperature $T(P_o)$, and retaining only the linear term, we have

$$L^{bb}[\lambda, T] = L^{bb}[\lambda, T(P_o)] + \frac{\partial L^{bb}[\lambda, T(P_o)]}{\partial T} [T - T(P_o)]. \quad (8)$$

This approximation is accurate to within 1% over the wavelength range from 10 to 13 μm and for a temperature range in excess of 10°K. This relationship allows Eq. (7) to be expressed as

$$T_{\Delta\lambda} = T(P_o) - [T(P_o) - \overline{T}_{\Delta\lambda}] k_{\Delta\lambda}{}^u, \quad (9)$$

where $T_{\Delta\lambda}$, $\overline{T}_{\Delta\lambda}$ and $k_{\Delta\lambda}$ are respectively the brightness temperature of the observed radiance, the equivalent brightness temperature of the atmosphere, and the atmospheric extinction coefficient, each averaged over the interval $\Delta\lambda$. Eq. (9) shows a linear relationship between brightness temperature and extinction coefficient, provided $\overline{T}_{\Delta\lambda}$ is approximately constant over the spectral region. A study by McMillin [3], and the results of the present study, show variations of less than 5 percent throughout the window region. Conceptually, therefore, measurements in only two wavelength intervals for which the respective absorption coefficients are significantly different are required to define the linear relationship.

Eq. (9) represents a two-channel algorithm for estimating SST and is represented graphically in Figure 1. For the wavelength intervals whose extinction coefficients are $k_{\Delta\lambda_1}$ and $k_{\Delta\lambda_2}$, the respective brightness temperatures $T_{\Delta\lambda_1}$ and $T_{\Delta\lambda_2}$ are measured. The intercept of the straight line connecting these two points and the ordinate is the surface temperature $T(P_o)$. To implement this algorithm the relative values of the extinction coefficients must be defined. In a previous study [2] these were obtained from radiative transfer models which have since been shown to be somewhat inaccurate. Therefore, before

an accurate demonstration of the procedure could be made it was necessary to modify the radiative transfer models and redefine the extinction coefficients.

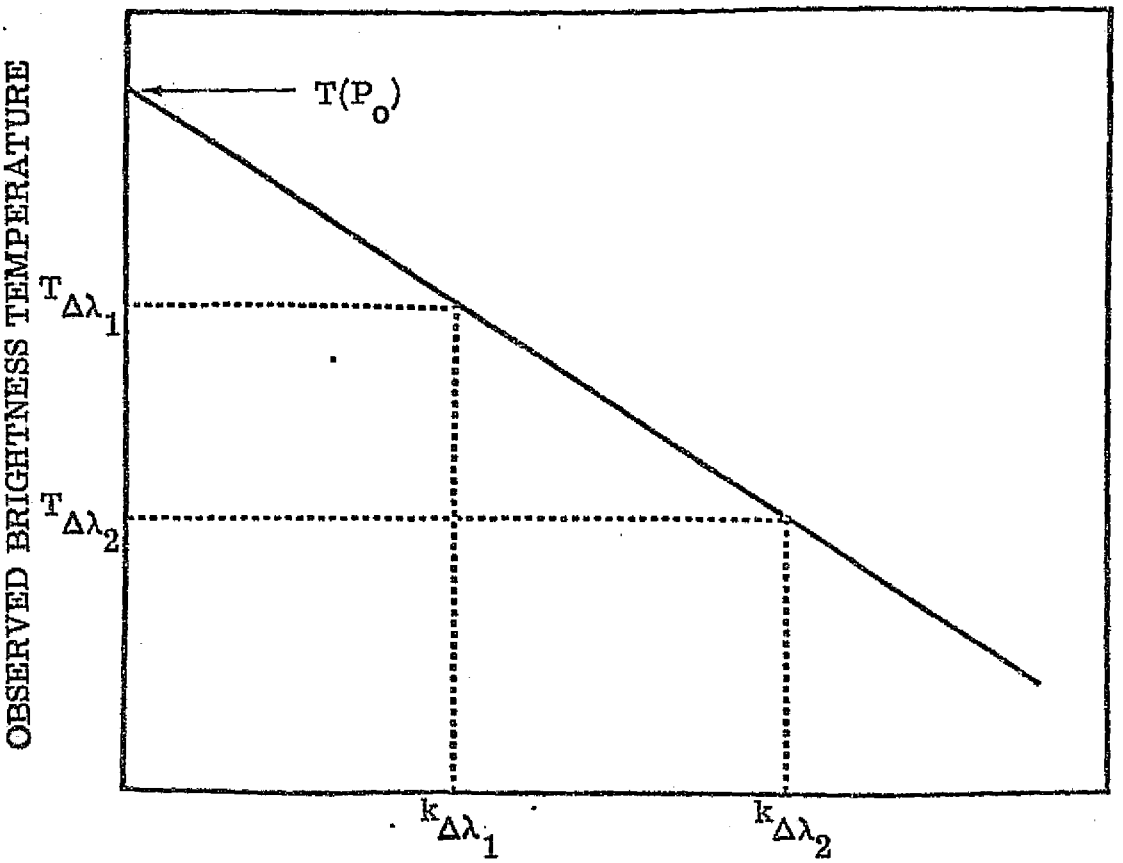

Figure 1. Graphical Representation of Two-Channel Algorithm

3

RADIATIVE TRANSFER MODEL MODIFICATION AND EXTINCTION COEFFICIENT REDEFINITION

The radiative transfer models used as a foundation for the SST algorithm development are discussed in detail by Anding [10]. Basically, the model numerically evaluates Eq. (3) accounting for the effects of molecular absorption and emission and the effects of aerosols on the atmospheric transmission. Molecular absorption is represented by band models, including all naturally occurring atmospheric molecules.

For the present investigation the required modifications were the development of new absorption models for H_2O local line absorption and H_2O continuum absorption throughout the spectral region from 8 to 14 μm.

Local line absorption was represented by the Goody model [11] which is given by

$$\tau_{\Delta\lambda} = \exp\left[\frac{-(S/d)u}{\sqrt{1 + \frac{2}{P}\frac{S}{2\pi\alpha}u}}\right], \tag{10}$$

where

S/d = intensity to line-spacing parameter for the interval $\Delta\lambda$ (cm^{-1})

$\frac{S}{2\pi\alpha}$ = intensity to half-width parameter for the interval $\Delta\lambda$ ($atm \cdot cm^{-1}$)

u = absorber thickness (pr. cm)

P = equivalent broadening pressure (atm) .

The parameters S/d and $S/2\pi\alpha$ were evaluated from a tabulation of spectral line parameters [12] using a procedure discussed by Goody [11], modified to account for an instrument slit function. The parameters were evaluated at a spectral resolution of 10 cm^{-1}, defined by the width of the slit function when the transmission is 50%. A comparison between band model and line-by-line derived spectra is shown in Figure 2. Observe that the transmission spectrum is well represented by the Goody model.

Continuum absorption in the window region results from two mechanisms; that caused by the wings of water vapor lines within the 6.3 μm and rotational water bands which are pressure broadened by foreign gases, and that caused by the same water vapor lines which are self

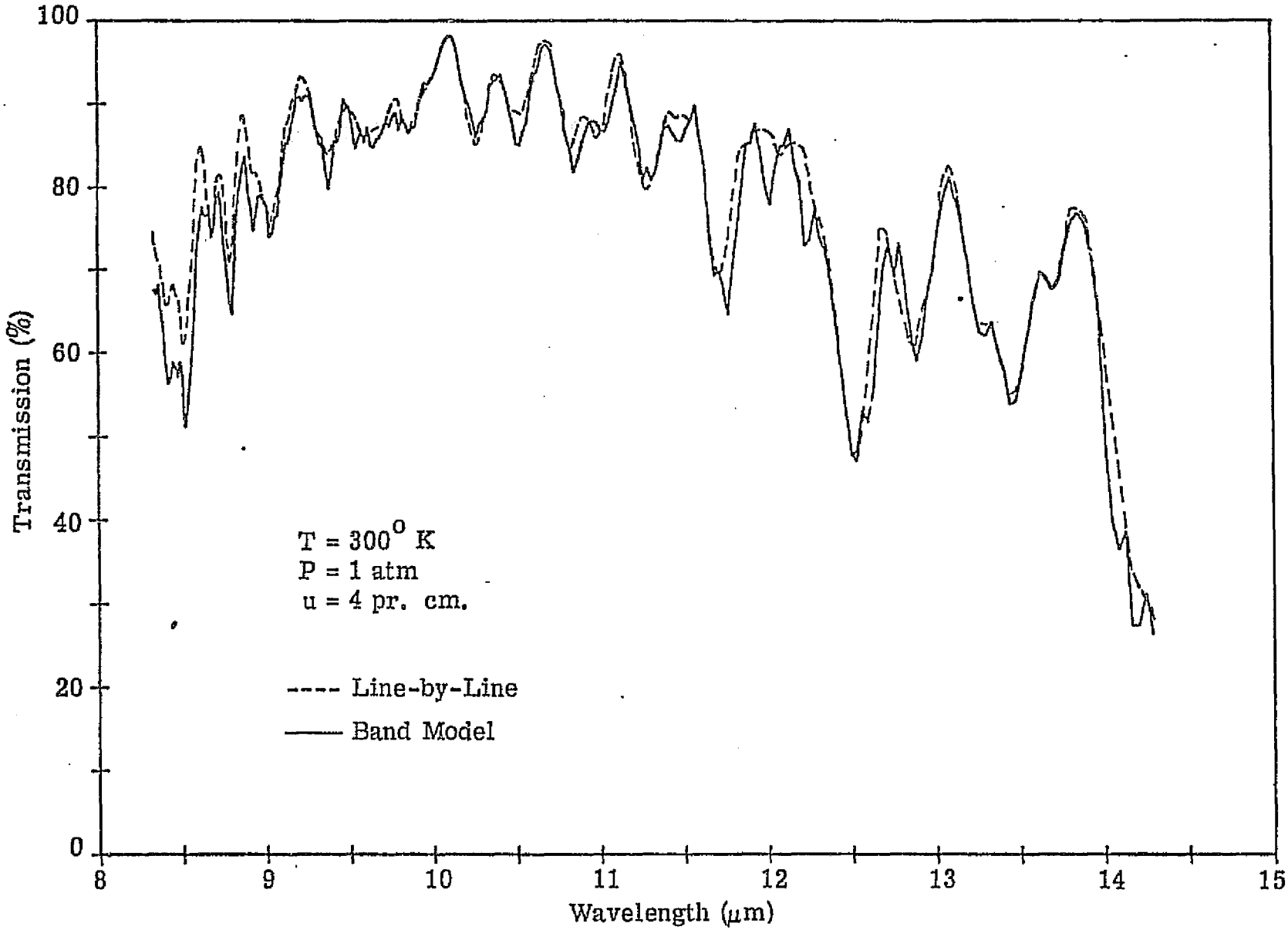

Figure 2. A Comparison of Band Model and Line-by-Line Derived Spectra for H_2O Local Line Absorption in the Infrared Window Region

broadened. The continuum absorption coefficient at total pressure P, and water vapor partial pressure p, is given by

$$C(P, p) = C_f P + C_s p \,, \tag{11}$$

where C_f is the absorption coefficient for foreign broadening at unit total pressure, and C_s is the coefficient for self-broadening at unit water vapor partial pressure.

The values of C_f and C_s adapted for the continuum model were based upon a subjective analysis of the data of Bignell [13], Burch [14], and McCoy [15]. The values adopted for C_s are illustrated in Figure 3. Discussions with Burch and Long indicated that a least-squares fit to the data would yield a self-broadening coefficient that was too high because of systematic errors for the larger data points and because of the consistency of the results of McCoy for the CO_2 laser line absorption at 10.59 μm. Therefore the selected values coincide with the lowest values shown.

The values adopted for C_f are based upon the 10.59 μm CO_2 laser measurements of McCoy [15]. McCoy measured the transmission as a function of total pressure for a fixed water vapor pressure. Using the self-broadening coefficient (C_s) as a basis, the foreign-broadening coefficient (C_f) was determined to be $0.005\, C_s$.

Both C_f and C_s are temperature dependent, the value of C_f increasing with increasing temperature and the value of C_s decreasing with increasing temperature. For self-induced absorption the dependence was adopted from the work of Bignell [13] at 2 percent per degree Kelvin. For foreign-induced absorption the temperature dependence was scaled from the temperature dependence of the rotational water lines, also at 2 percent per degree Kelvin.

Upon completion of the model revisions the algorithm extinction coefficients were redefined. Three wavelength intervals within the

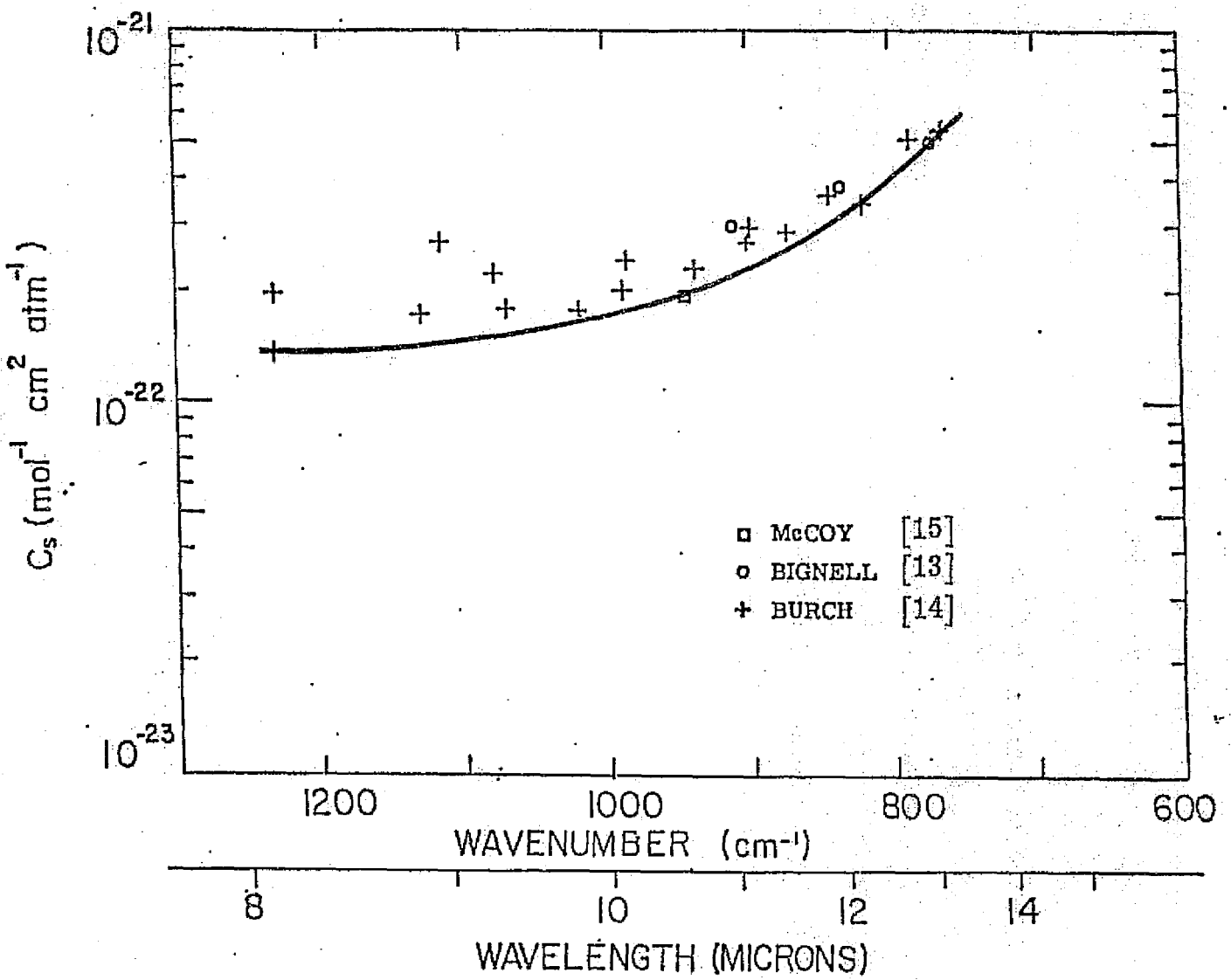

Figure 3. H_2O Self-Broadening Continuum Absorption Coefficient for Infrared Window Region at 296° K.

window region between 10 and 13 μm were chosen, rather than only two, to observe possible nonlinearities between brightness temperature and extinction coefficient. The intervals chosen were those used by Prabhakara [4], and are respectively, 10.25 - 11.25, 11.25 - 12.0, and 12.0 - 12.9 μm. This result is a consequence of selecting a 1 μm wide interval beginning at the long wavelength side of the 9.6 μm ozone band (the most transparent part of the window region) and then dividing the remaining wavelength interval into two equal wavenumber segments, each 56 cm^{-1} wide.

The mean extinction coefficient for each interval was redefined empirically from transmission spectra computed from the modified version of the radiative transfer model. The empirical procedure was as follows. Ten atmospheric representations of temperature and humidity were selected from the NASA Four-Dimensional Model Atmosphere compilation [16], representing moist and dry conditions ($\pm$ one standard deviation from mean moisture conditions) for five oceanic global regions extending from the North Sea to the equator. These atmospheres were selected so that the complete range of atmospheric temperature and humidity conditions occurring over the worlds oceans would be represented. These atmospheric data were input to the radiative transfer model and spectral transmission from 10 to 13 μm was computed. These values were integrated over the respective wavelength intervals and transmission versus effective absorber thickness was plotted. The result is presented in Figure 4. Assuming transmission is accurately represented by Beers Law, i.e., $\tau = \exp(-ku)$, linear least squares fits to $\ell n \tau$ versus u yielded three respective values for the extinction coefficient, which are also given in Figure 4.

To demonstrate the relationship between brightness temperature and extinction coefficient using actual data, the ten model atmospheres were input to the radiative transfer models and the vertical upwelling

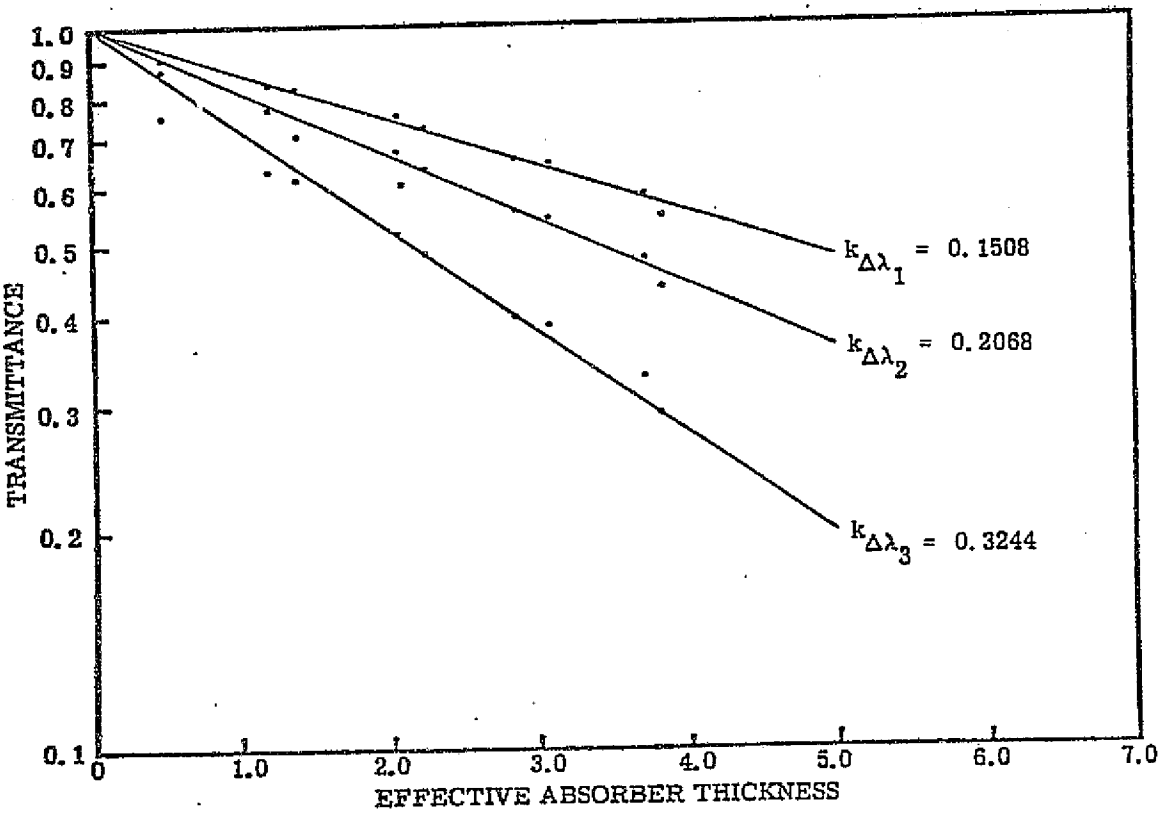

Figure 4. Average Transmission Versus Effective Absorber Thickness for Three Wavelength Regions (10.25 - 11.25, 11.25 - 12.0, 12.0 - 12.9 μm). $k_{\Delta\lambda_1}$, $k_{\Delta\lambda_2}$ and $k_{\Delta\lambda_3}$ are Beers Law Extinction Coefficients for the Respective Wavelength Intervals Denoted by $\Delta\lambda_1$, $\Delta\lambda_2$ and $\Delta\lambda_3$.

radiance at space altitudes, emanating from a sea surface whose temperature equaled $T(P_o)$ was calculated. Two aerosol representations were selected for the computations taken from the work of Fenn [17];* one whose optical properties and size distribution were consistent with a 100 percent maritime haze and the other with a 60 percent maritime haze and a 40 percent continental haze. The altitude distribution of aerosol density was assumed variable and controlled by the sea-level visibility. A 23 km visibility was used for the maritime haze, a 10 km visibility for the maritime-continental haze. The calculations of radiance were made by numerically evaluating Eq. (3), using the water vapor transmission models described previously to evaluate $d\tau(\tau, P)$. For each of the twenty spectra, in-band brightness temperatures were evaluated and plotted versus extinction coefficient. The results are shown in Figure 5a-5e. The straight lines are least squares fits to the data.

Observe that a nonlinearity exists between brightness temperature and extinction coefficient, which diminishes at higher brightness temperatures. This occurs because the atmospheric brightness temperature increases approximately 5 percent at the longer wavelength regions, and the increase is observable at the lower surface temperatures, but becomes nearly insignificant for surface temperatures above 295^{o} K. Also note that the atmosphere causes a decrease in the observed brightness temperature of the sea surface ranging from 2^{o} K for the cool northern region to greater than 5^{o} K for the warm equatorial region. The application of the SST technique to these data does, however, estimate input SST values to within $\pm 0.5^{o}$ K. Furthermore, the 3-band estimate is insignificantly better than the 2-band estimate ($\pm 0.5^{o}$ K compared to $\pm 0.3^{o}$ K).

---

* Based upon extensive measurements and analyses, Fenn has assembled a compendium (to be published) of aerosol properties for different geographic regions. Descriptors include extinction and scattering coefficients, size distribution, refractive index, and density versus altitude.

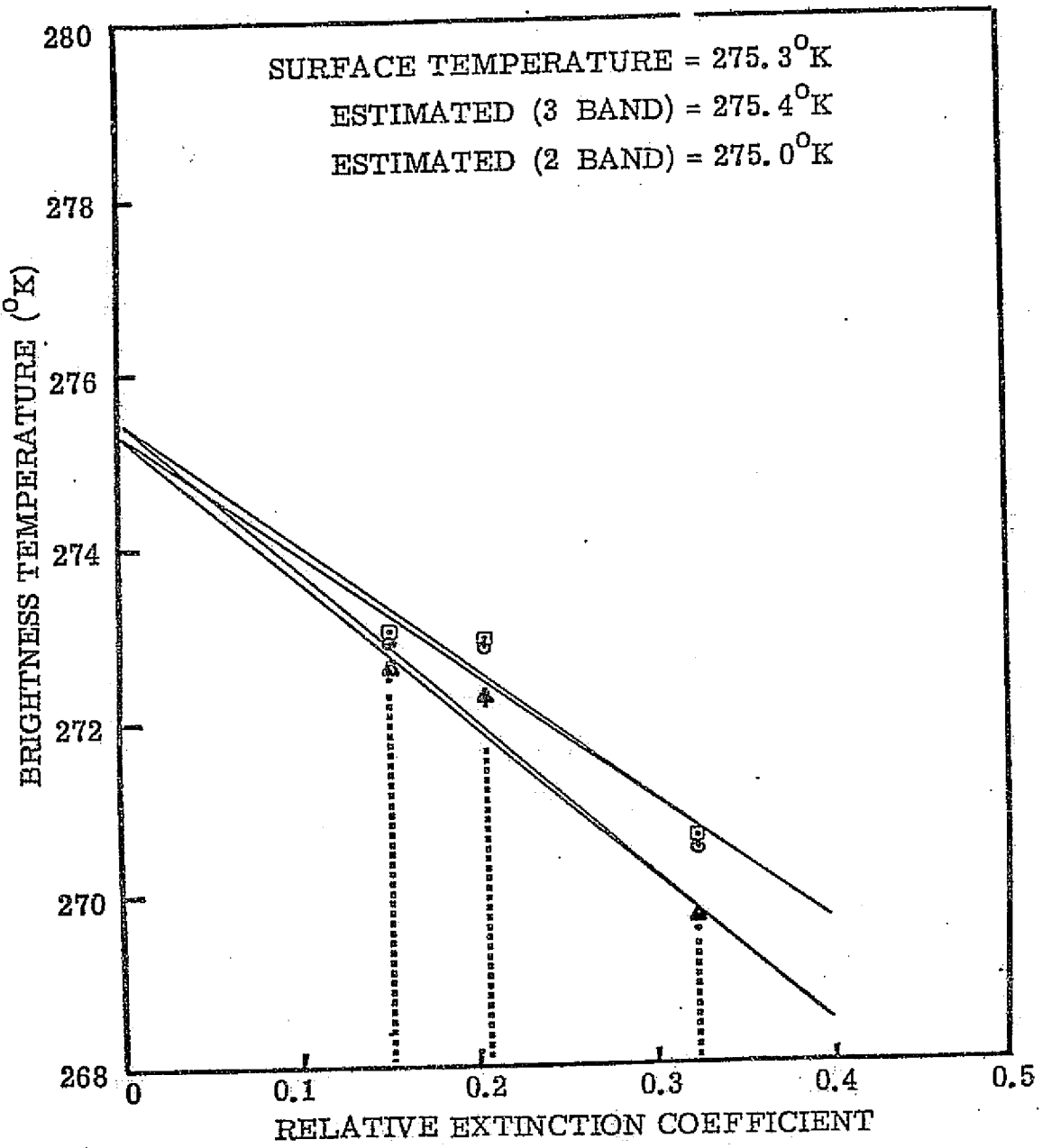

Figure 5a. Brightness Temperature Versus Extinction Coefficient.
Key: ⊡ Low Humidity, Continental-Maritime Haze;
⊙ Low Humidity, Maritime Haze;
▲ High Humidity, Continental-Maritime Haze;
• High Humidity, Maritime Haze.

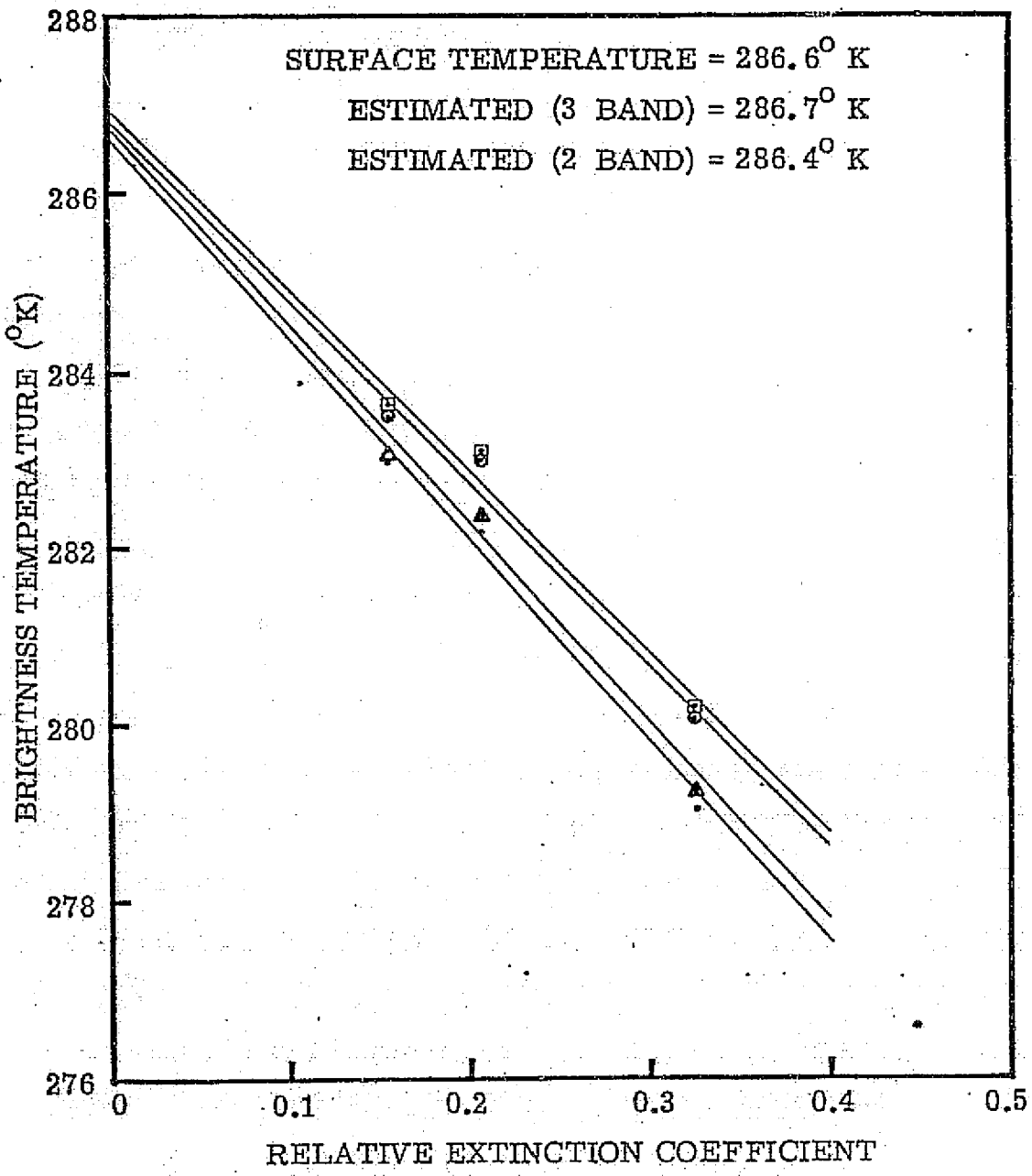

Figure 5b. Brightness Temperature Versus Extinction Coefficient.
Key: ⊡ Low Humidity, Continental-Maritime Haze;
⊙ Low Humidity, Maritime Haze;
▲ High Humidity, Continental-Maritime Haze;
• High Humidity, Maritime Haze.

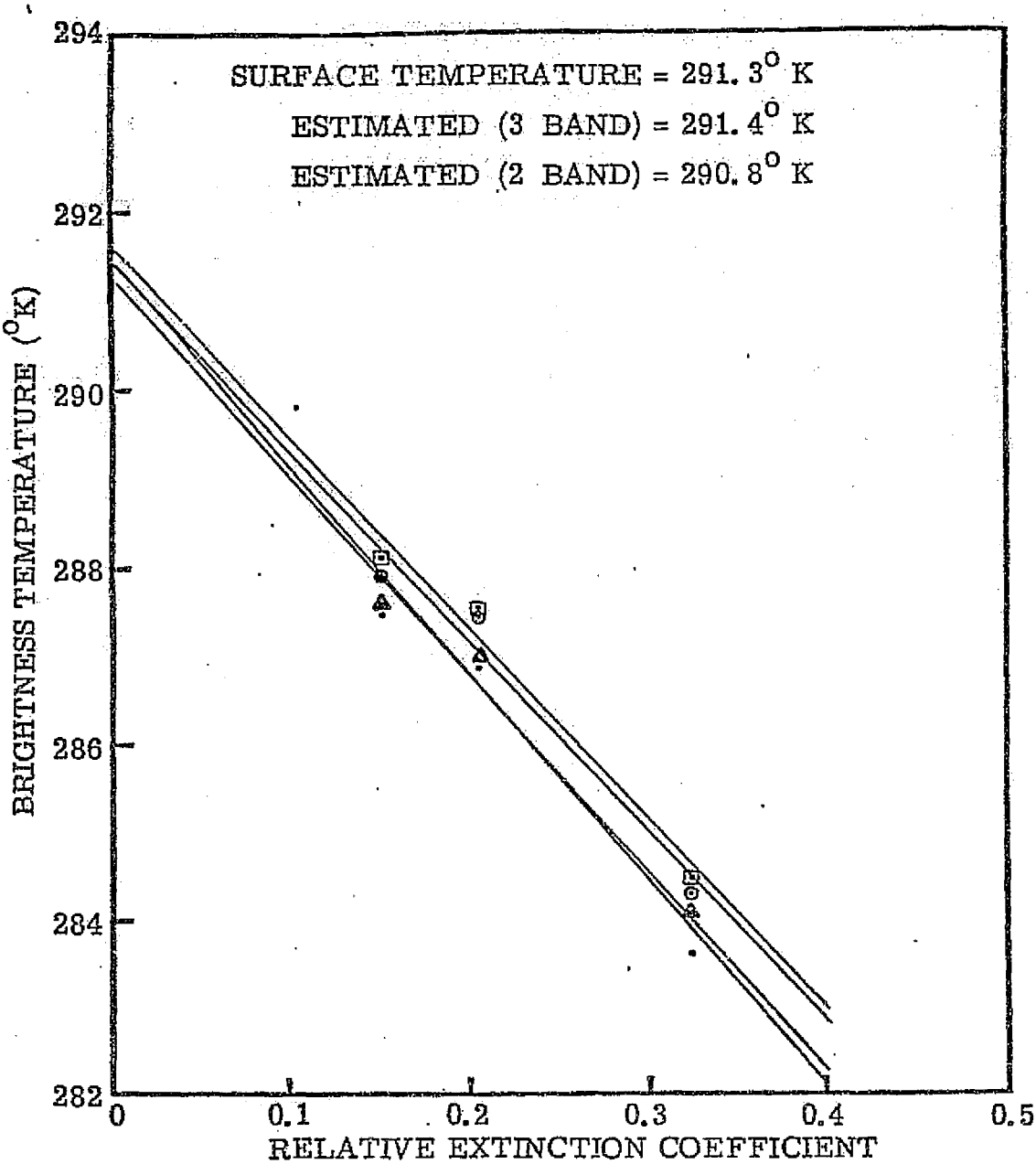

Figure 5c. Brightness Temperature Versus Extinction Coefficient.
Key: ⊡ Low Humidity, Continental-Maritime Haze;
⊙ Low Humidity, Maritime Haze;
△ High Humidity, Continental-Maritime Haze;
· High Humidity, Maritime Haze.

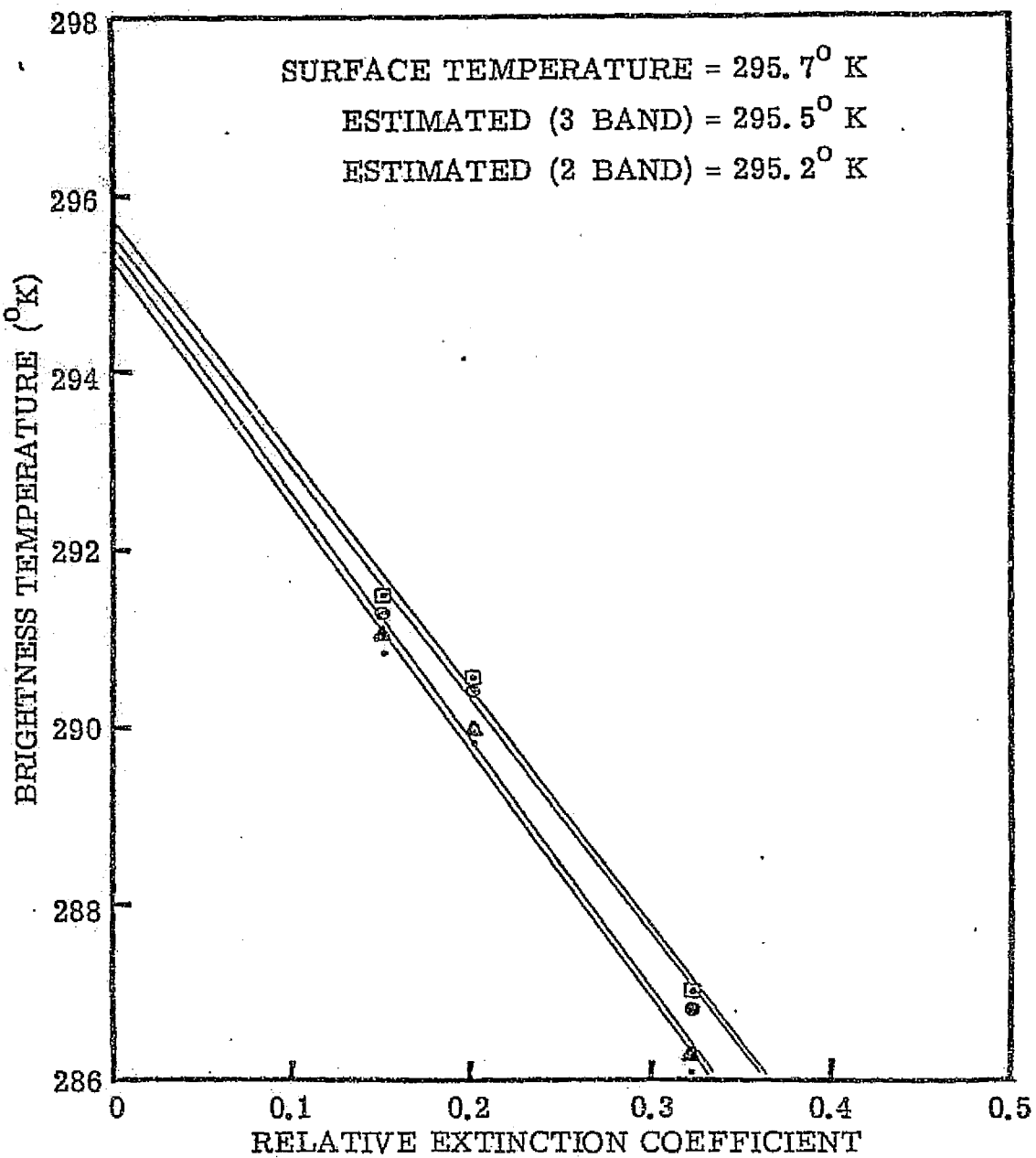

Figure 5d. Brightness Temperature Versus Extinction Coefficient.
Key: ⊡ Low Humidity, Continental-Maritime Haze;
⊙ Low Humidity, Maritime Haze;
△ High Humidity, Continental-Maritime Haze;
. High Humidity, Maritime Haze.

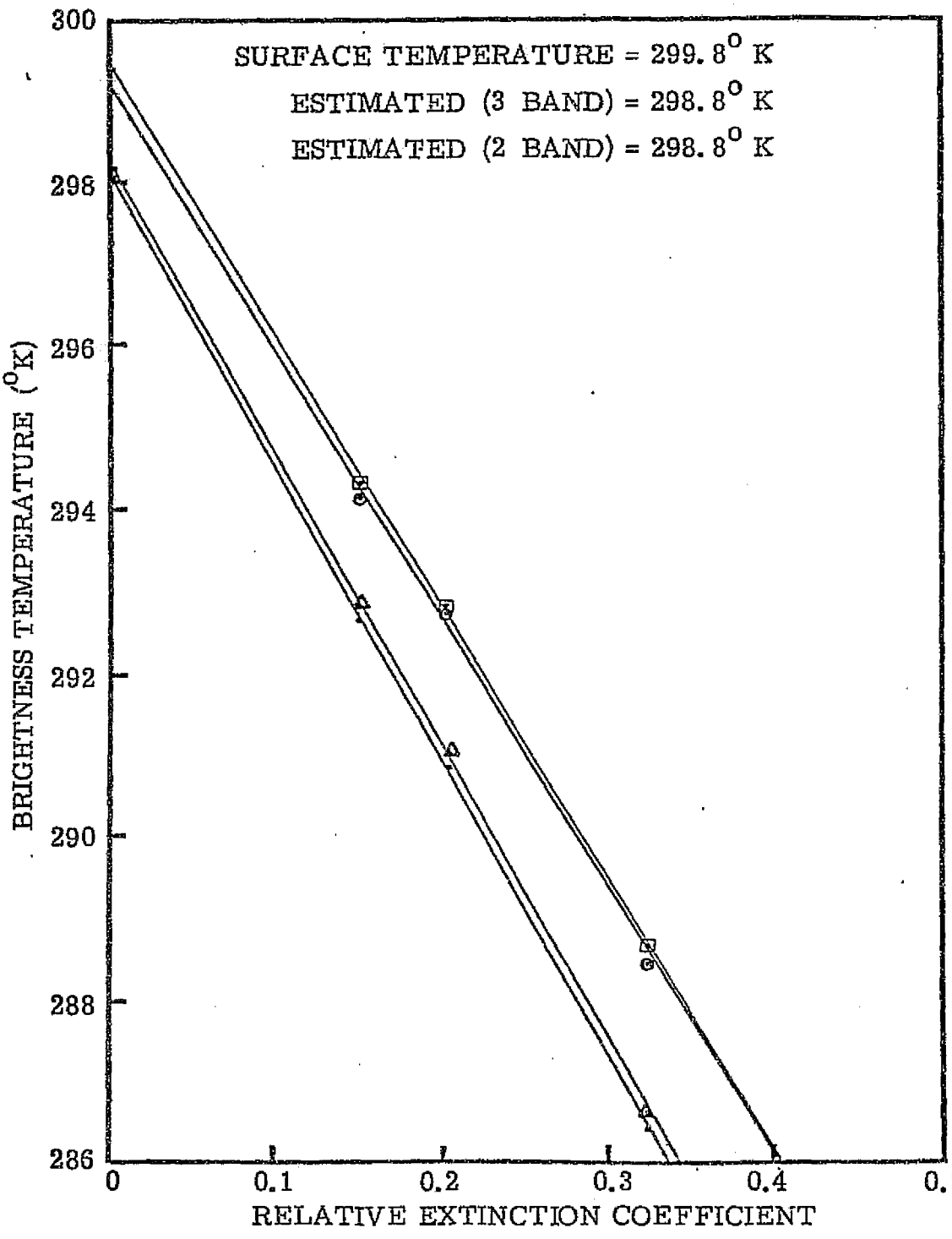

Figure 5e. Brightness Temperature Versus Extinction Coefficient.
Key: ⊡ Low Humidity, Continental-Maritime Haze;
⊙ Low Humidity, Maritime Haze;
▲ High Humidity, Continental-Maritime Haze;
. High Humidity, Maritime Haze.

PRESENTATION OF RESULTS

The application of the SST algorithm to actual space-acquired data was first performed on data measured by the IRIS instrument on Nimbus 4. The instrument is a Michelson interferometer sensitive to radiation in the spectral range from 5 to 25 μm at a spectral resolution of 2.8 cm^{-1}. The instrument is positioned vertically and its 2.5° half-angle circular f. o. v. views an area on the earth's surface approximately 94 km in diameter from the nominal satellite altitude of 1100 km. Figure 6 displays an IRIS spectrum compared to a spectrum computed by the radiative transfer model. The spectral region of concern extends from approximately 800 to 1000 cm^{-1}.

A selection of six IRIS spectra were selected from the archived data over cloud-free ocean areas and the mean brightness temperature for each one of the three chosen spectral intervals was calculated. These data, taken from Prabhakara [4], were plotted versus relative extinction coefficient and the results shown in Figures 7 and 8. Observe nearly perfect linearity is demonstrated and that excellent agreement is obtained between predictions and ship measurements for three of the cases (Figure 7). The reason for the discrepancy for the other three cases (Figure 8) is unknown, although it could be attributable to a decrease in surface emissivity resulting from a high sea state. It is felt, however, that the results are very encouraging.

The utilization of Skylab EREP S191 data as a verification experiment fell far short of expectations because of instrument problems. Although the problems have been identified, their effects remain uncorrected. A circumstance of the spectrometer was that inaccurate data resulted whenever the brightness temperature of the spectral radiance was significantly different than either the ambient calibration source temperature, or the temperature of the internal mirrors or dichroic. Of the eight test areas planned for analysis this condition existed for all but two; the Monroe Reservoir on 10 June 1975 and Key West on 8 January 1974. Although a large effort was expended for each test site in acquiring and processing ground and air-truth

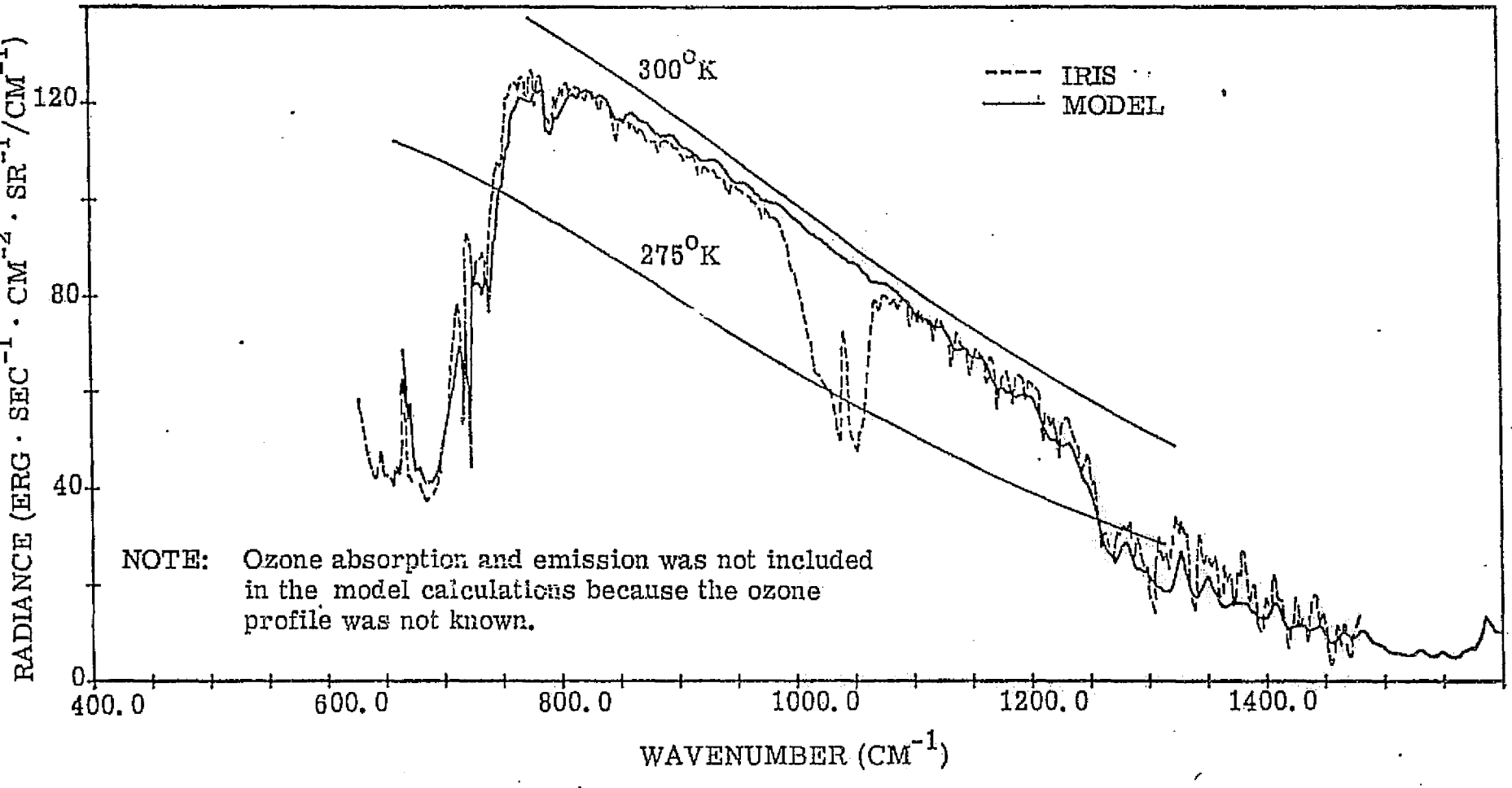

Figure 6. Comparison of Radiative Transfer Model Computations with IRIS Data

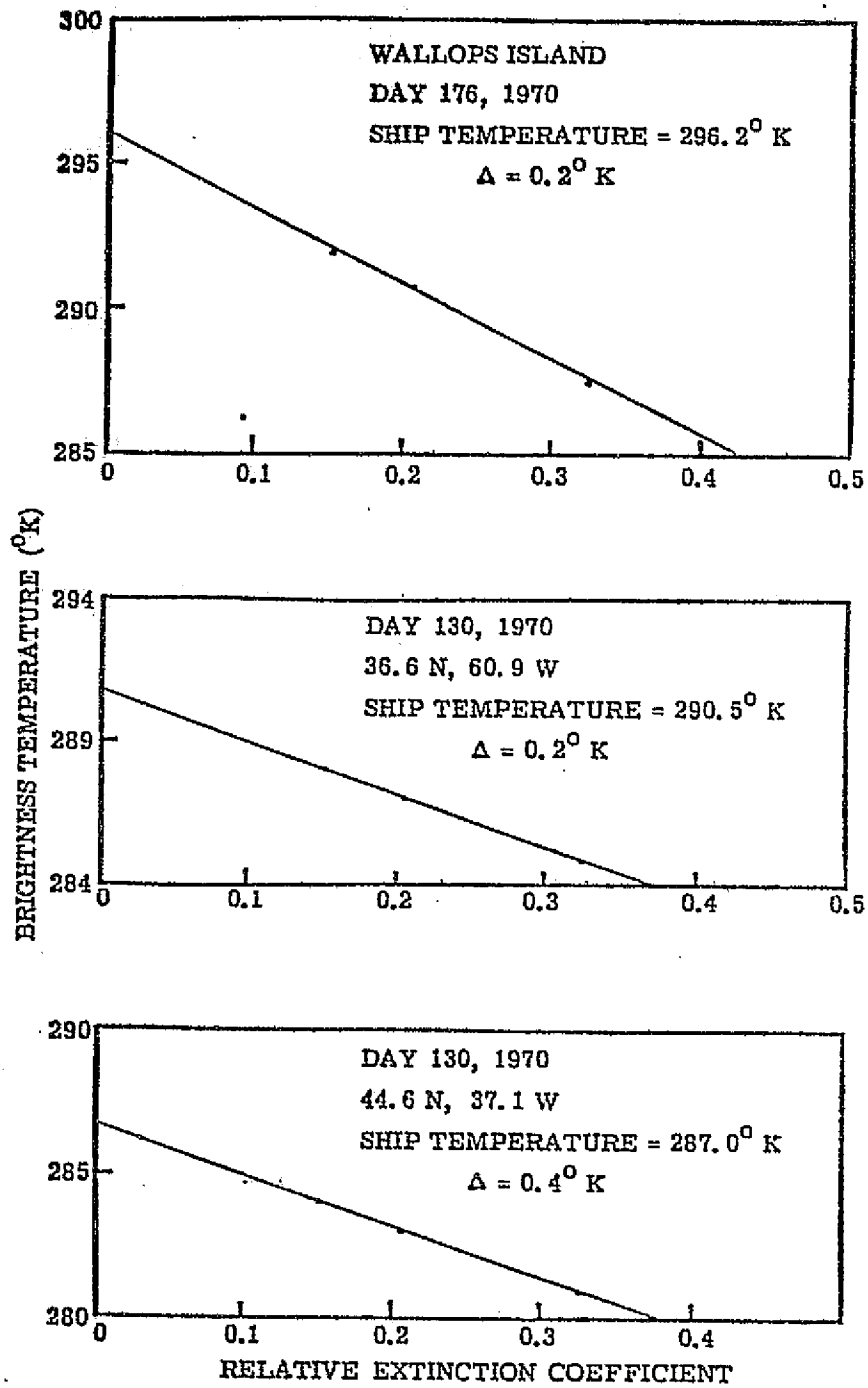

Figure 7. IRIS Measured Brightness Temperature Versus Relative Extinction Coefficient

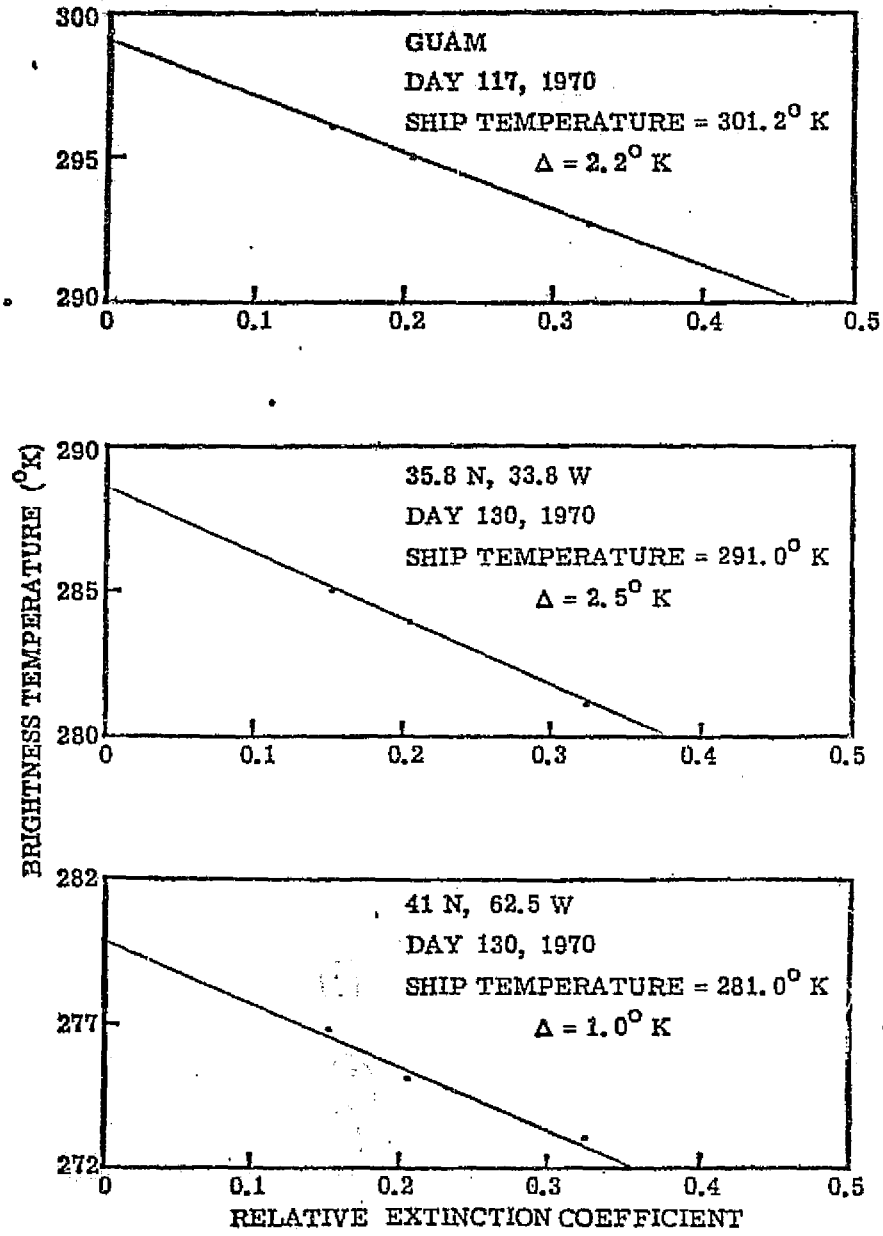

Figure 8. IRIS Measured Brightness Temperature Versus Extinction Coefficient

data, and in processing and analyzing the radiance data, only data for the two previously mentioned test sites were useful. The data from these missions are presented and discussed herein. All other data have been discussed previously [9] and are not reported here. As indicated in reference 9, the data for EREP Pass 8 (11 June 1973) and EREP Pass 87 (21 January 1974) were scheduled for analysis. Unfortunately, the data for Pass 8 were contaminated by clouds and the data for Pass 87 suffered from severe calibration errors; both data sets were therefore unusable.

4.1 Key West, 8 January 1974, EREP Pass 78

The data for this test site were the most comprehensive of all test sites planned for analysis. In addition to the S191 spectra, ground and air-truth data were acquired which consisted of radiometric surface temperatures, bucket temperatures, and radiosonde data. The test site, a clear patch of ocean at approximately 24.25 N and 81.7 W, was acquired approximately 45° forward of the spacecraft at 16:29:54 GMT and tracked to nadir at 16:30:52 GMT. During that time 62 spectra were acquired. The main thrust of the analysis performed on these and other measurement data was to verify the radiative transfer models by comparison of measured and calculated spectra, and to test the SST algorithm using both measured and calculated data. It was hoped that the decrease in radiance with an increase in nadir observation angle (because of increased atmospheric absorption and smaller path radiance) would be an observable phenomena. This decrease equals approximately 10 $\mu w/cm^2$-sr-μm as the nadir angle is increased from 0° to 45°. Because the instrument noise level (see Figure 10) equalled approximately 10 $\mu w/cm^2$-sr-μm, the experiment was not sensitive to this phenomena. Consequently, all data were assumed to have been taken at a nadir angle of 34° (i.e., the approximate angle at which the optical depth increased by 50% of the increase which occurs at 45°).

The initial step in the analysis was to check for calibration errors resulting from a drift in sensor responsivity after pre-pass calibration. This was achieved by computing the average spectral radiance for 30

sequential scans of the ambient calibration source (during the post-pass autocal sequence) and comparing the results with a blackbody radiance spectrum evaluated at the temperature of the ambient calibration source (obtained from the housekeeping data). The result is shown in Figure 9. The calibration source temperature at the time of the post autocal sequence was determined to be 291.67°K. The best fit blackbody curve for the post autocal radiance was determined to be 290.81°K, 0.86 degrees less. The lapsed time between the pre-pass calibration and the post-pass autocal was 1 hour and 30 minutes and data acquisition occurred 30 minutes after pre-pass calibration. Assuming the total difference is caused by a linear responsivity drift, the correction required is only approximately 0.3°K. In the context of the present experiment this is a negligible amount.

The next step in the analysis was to quantify the random fluctuations in the observed spectral data and compare them with the predicted NESR of the instrument. This was achieved by computing the standard deviation of radiance at each wavelength for the 62 measured spectra. Spectral values of standard deviation are plotted and compared with the instrument NESR in Figure 10. Since variations in atmospheric absorption and emission, and variations in sea surface radiations all contribute to the variance in the observed S191 signal, the system noise level appears commensurate with predictions.

A test of the radiative transfer model was accomplished by calculating the spectral radiance one would expect at the entrance aperture of the S191 spectrometer, based upon the measured values of SST and atmospheric humidity and temperature. The specific support data acquired for EREP Pass 78 were:

1) PRT-5 SST acquired at an altitude of 1500 feet.
2) Bucket temperatures.
3) Radiosonde data giving temperature and humidity data to the 300 mb pressure level.
4) ITOS Vertical Temperature Profile Radiometer (VTPR) data giving temperature and humidity data to the 400 mb pressure level.

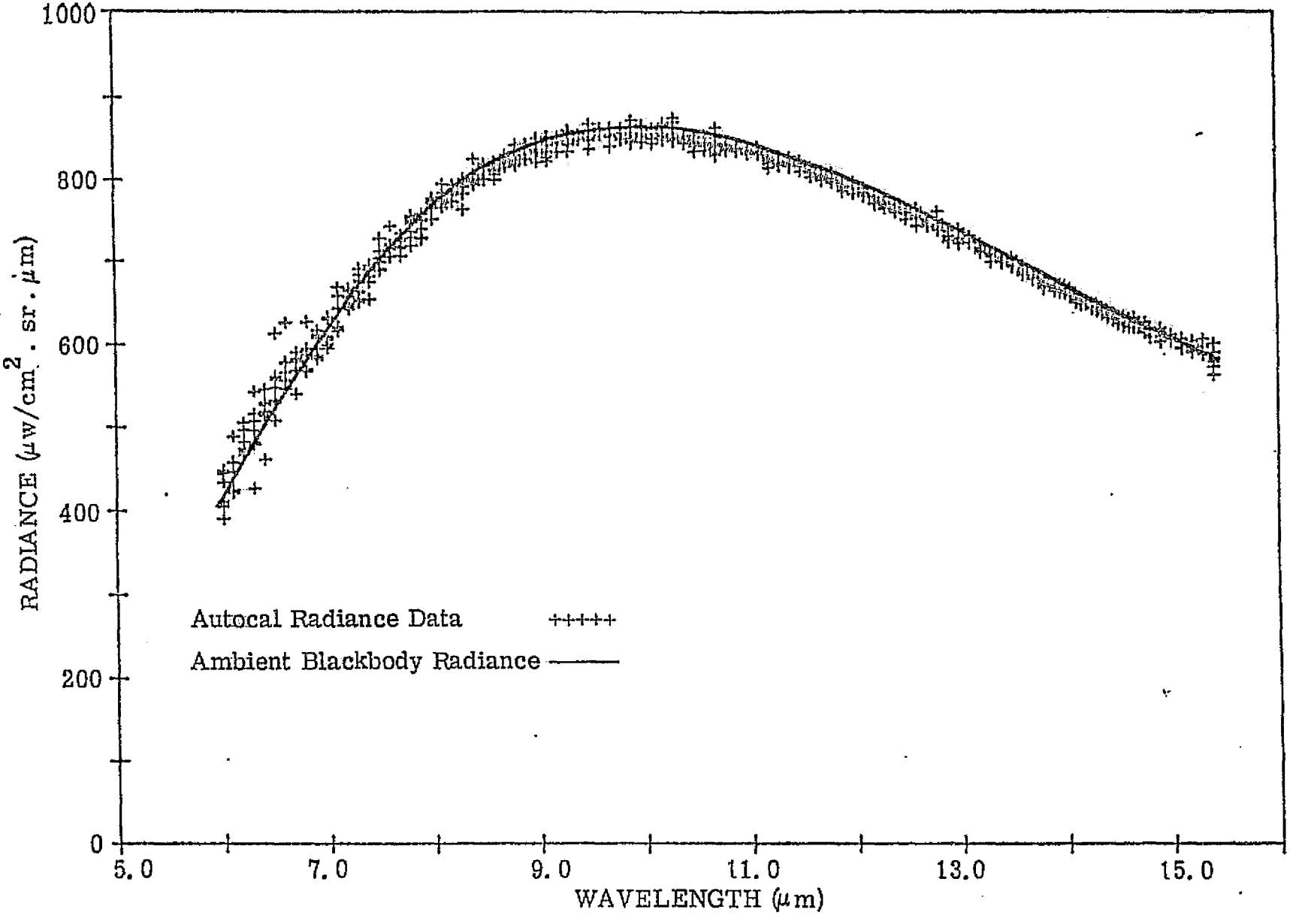

Figure 9. Comparison of Autocal Radiance Data with Ambient Blackbody Radiance for a Blackbody Temperature of 291.67° K.

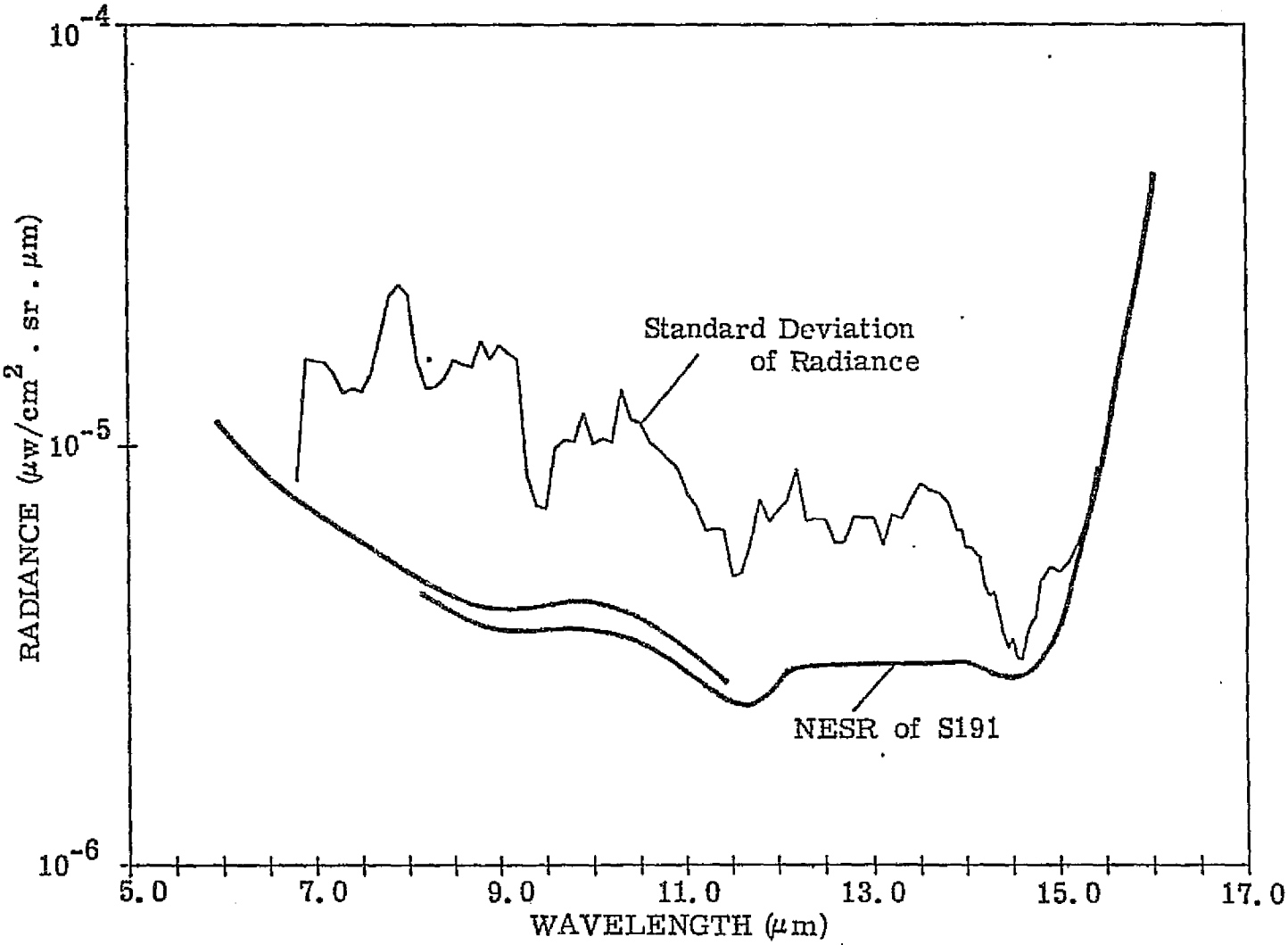

Figure 10. Standard Deviation of Radiance Compared to NESR of S191 Spectrometer for SL-4, Pass 78.

The radiosonde and VTPR data were processed and analyzed and a representative model atmosphere was constructed. The temperature and humidity profiles are shown in Figures 11 and 12, respectively. The actual radiosonde and VTPR data are given in Tables 1 and 2, respectively. The PRT-5 radiometric SST's and bucket temperatures were obtained by NOAA and are shown in Figure 13. The large difference between radiometric and bucket temperatures is not known at the present time.

The remaining step in the analysis was to use the model atmosphere data and the SST data and calculate the spectral radiance at the entrance aperture of the S191 for comparison with measured data. To make the comparison as realistic as possible the effects of aerosols were included. Since aerosol support data were not acquired, these data were assumed. They were a 100% maritime haze with a 23 km sea level visibility. The actual extinction coefficients were taken from the work of Fenn [17]. Radiance computations were performed for a SST of 296° K and a surface emissivity of 0.99. The result is given in Figure 14. Observe that the agreement is excellent from approximately 11 to 13 μm, but shows significant differences in other spectral regions. For wavelengths short of 10 μm the low measured values are probably caused by the previously mentioned calibration problem because aperture brightness temperatures for wavelengths shorter than 10 μm are less than the ambient calibration source temperature. The small difference at the long wavelength side of the 9.6 μm ozone band (the measured values are slightly lower than the calculated values) is probably caused by a lower instrument spectral resolution than that of the calculated values.

To examine the application of the SST estimation technique to these data, for both the S191 spectra and the model calculations, the in-band brightness temperatures were computed and plotted versus relative extinction

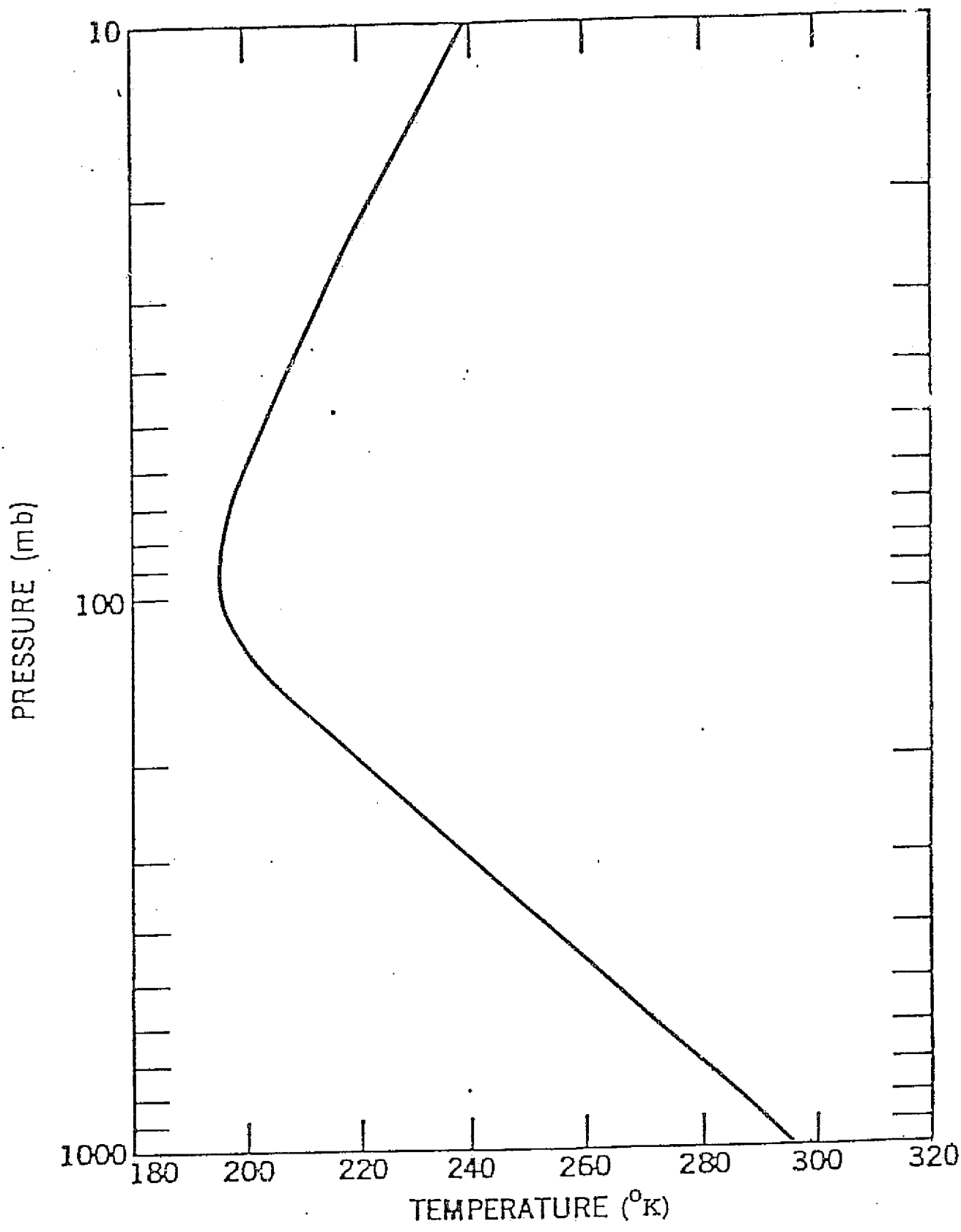

Figure 11. Atmospheric Temperature for Key West on 8 Jan 74.

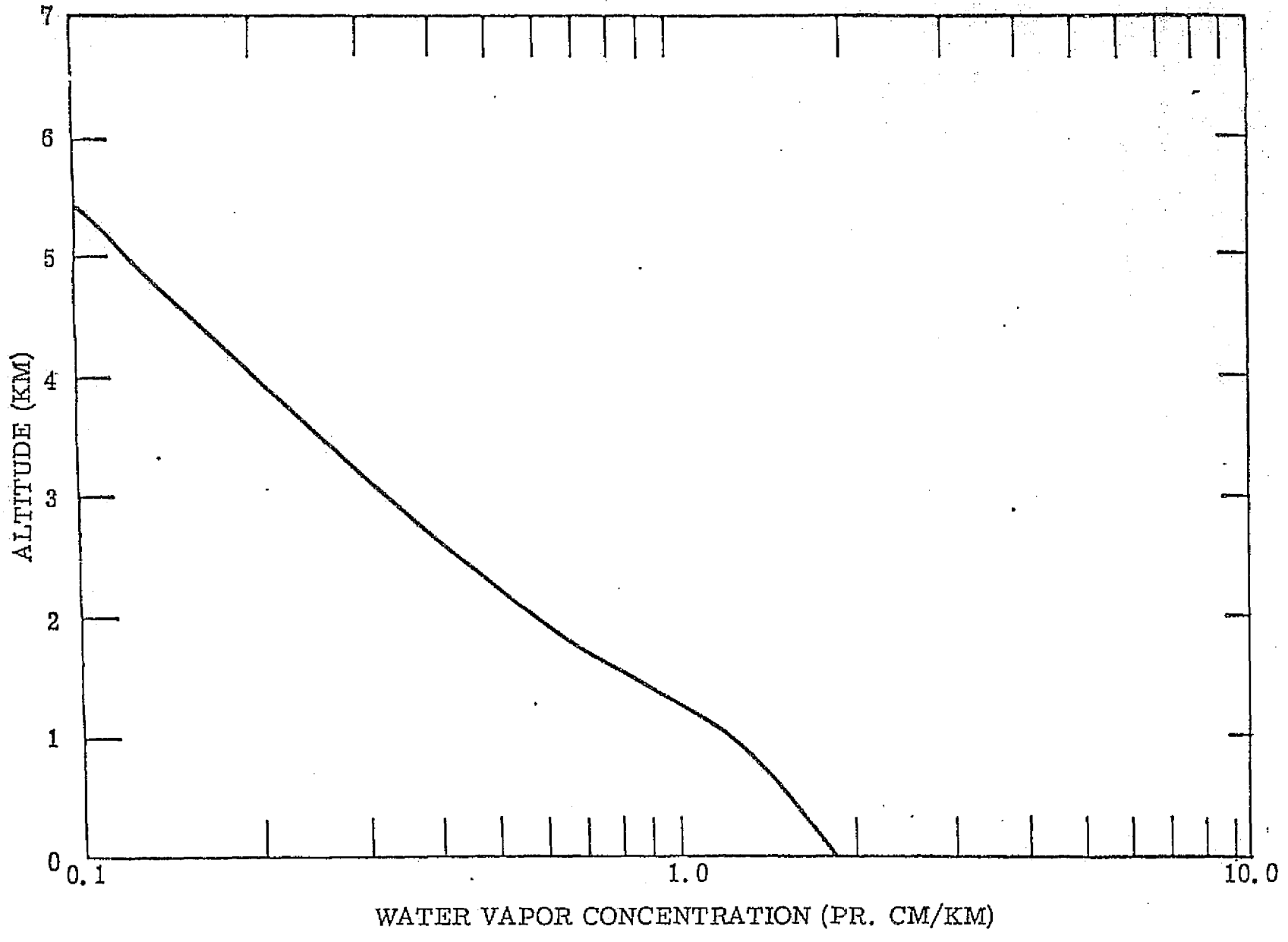

Figure 12. Water Vapor Concentration for Key West on 8 Jan 74.

Table 1.

Radiosonde Data for Key West on 8 Jan 74
Latitude = 24.6N Longitude = 81.7W

H(m)	P(mb)	T(K)	R.H.(%)
0.0	1021.0	298.0	79.0
83.2	1011.0	294.8	82.0
175.4	1000.0	296.2	85.0
1035.9	902.0	290.3	86.0
1342.8	869.0	289.1	63.0
1523.8	850.0	288.3	64.0
1935.9	808.0	286.0	66.0
2026.4	799.0	285.4	34.0
2138.2	788.0	284.4	72.0
2282.4	774.0	283.1	66.0
2641.5	740.0	281.5	72.0
2837.0	722.0	281.7	30.0
3081.5	700.0	281.0	31.0
3413.5	671.0	278.4	55.0
3781.5	640.0	276.5	42.0
4014.3	621.0	276.3	22.0
5216.6	530.0	266.9	21.0
5649.8	500.0	263.8	13.0
6104.6	470.0	255.8	10.0
7553.6	384.0	248.3	14.0
9250.4	300.0	234.1	14.0
10453.8	250.0	224.3	0.0
11159.3	224.0	222.9	0.0
11510.6	212.0	224.3	0.0
11882.5	200.0	222.9	0.0
13719.2	150.0	210.6	0.0
16309.7	100.0	196.1	0.0
18590.3	70.0	197.5	0.0
18966.6	66.0	198.0	0.0
19470.7	61.0	201.7	0.0
19793.3	58.0	200.5	0.0
20250.7	54.0	205.6	0.0
20744.2	50.0	205.4	0.0
21421.8	45.0	208.5	0.0
21714.9	43.0	215.1	0.0
24050.5	30.0	222.0	0.0
25791.3	23.0	226.9	0.0
26712.9	20.0	225.8	0.0
27789.6	17.0	225.2	0.0
28192.6	16.0	225.0	0.0
29326.3	13.5	229.3	0.0

Table 2.

VTPR Data for Key West on 8 Jan 74
Latitude = 23.98N Longitude = 80.78W

P(mb)	T_{air}(K)	T_{dew}(K)	P_{H_2O}(mb)
1000	298.12	294.87	25.96
850	288.35	285.37	14.21
700	279.06	271.77	5.51
500	262.62	252.79	1.21
400	250.90	240.58	0.40
300	236.07	-	-
250	227.39	-	-
200	219.79	-	-
150	212.73	-	-
100	207.04	-	-
70	199.43	-	-
50	206.10	-	-
30	217.36	-	-
20	222.16	-	-
10	229.47	-	-

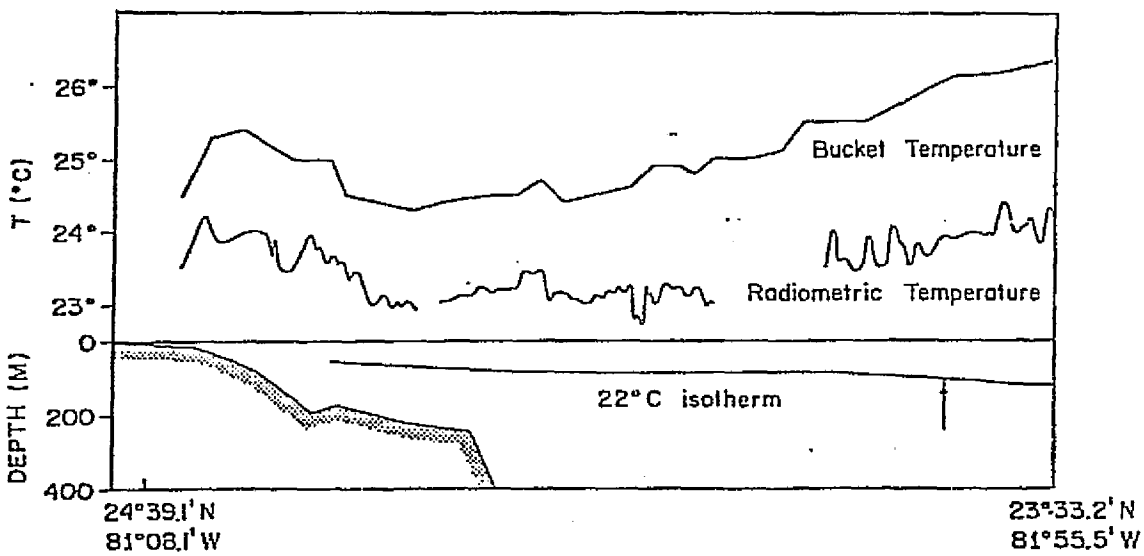

Figure 13. Sea Temperature Data from NOAA for Key West on 8 Jan 74.

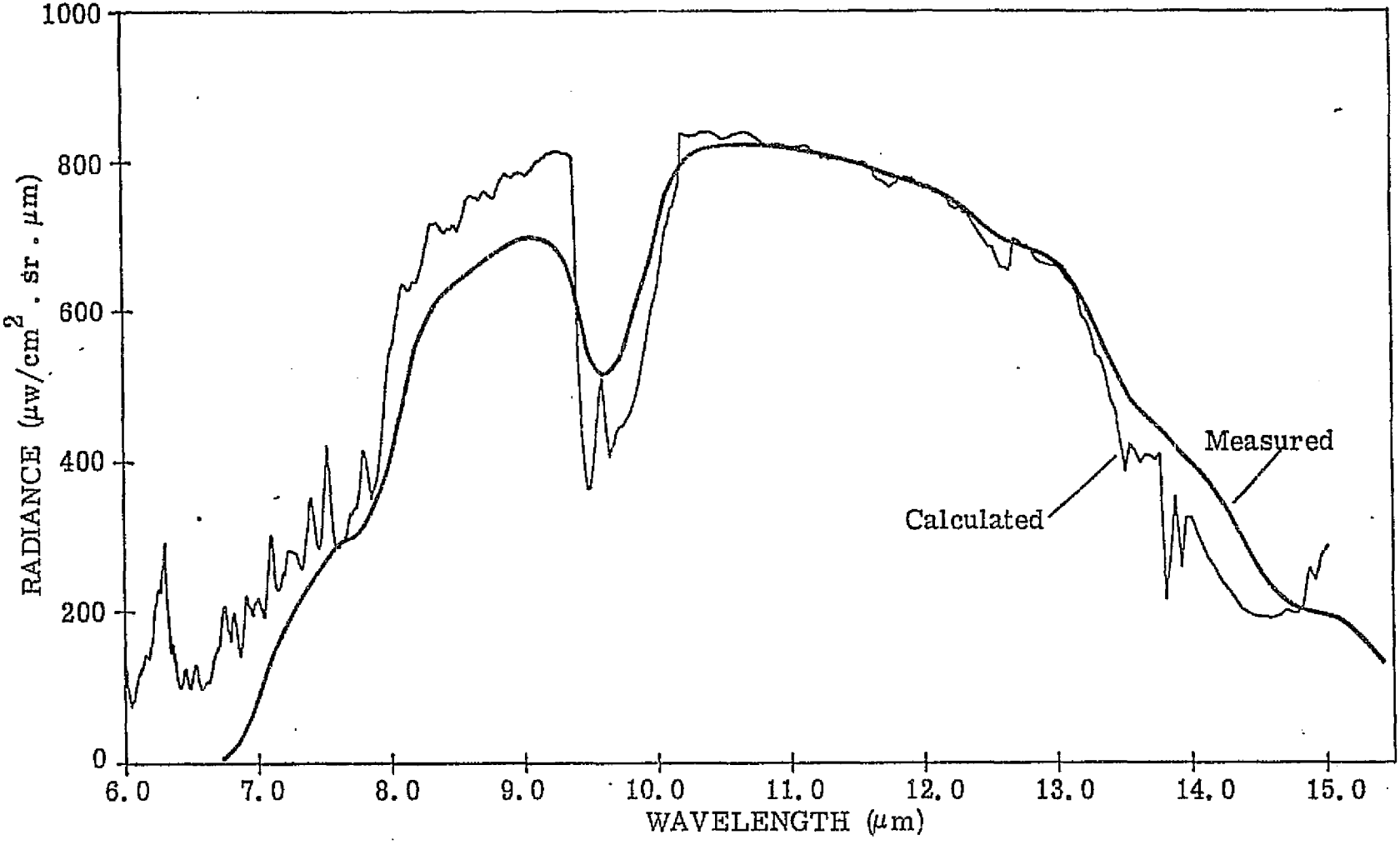

Figure 14. Comparison of Measured and Calculated Spectral Radiance for Key West on 8 January 1974. SST = 296^{o} K, ϵ = 0.99.

coefficient. Least squares lines were fitted to the data and the results are shown in Figure 15.

The close agreement between model and measurement predictions of SST, and the near-linear relationship of brightness temperature with relative extinction coefficient is as predicted. Note that the effect of the atmosphere on the observed brightness temperature in the most transparent region of the window is approximately $7^{o}K$, demonstrating the need to compensate atmospheric effects for accurate SST measurement. The reason for the discrepancy of $2^{o}K$ between predictions and PRT-5 measurements is unknown, however, there is a possible explanation other than measurement error or errors in the estimation technique. Since the Data Acquisition Camera was not operating during the EREP overpass the gimbal angles for the S191 are not known and hence, the precise location of the S191 field-of-view is unknown. The distance between the location of the radiometric SST measurements and the sub-orbital track was about 16 miles. Therefore, it is possible that the surface truth data were obtained for a different location than that measured by EREP and the actual SST is more nearly $294^{o}K$ than $296^{o}K$.

4.2 Monroe Reservoir, 10 June 1973, EREP Pass 7

The Monroe Reservoir was not a selected test site for this investigation but because of the lack of usable data from the planned sites, and because the data appeared accurate, it was processed and analyzed. S191 data were acquired for the central portion of the reservoir between approximately 14:26:02 and 14:26:09 GMT. The gimbal angles at the time of acquisition were 05 down and 03 left. The seven spectra acquired were averaged and placed in readiness for further analysis.

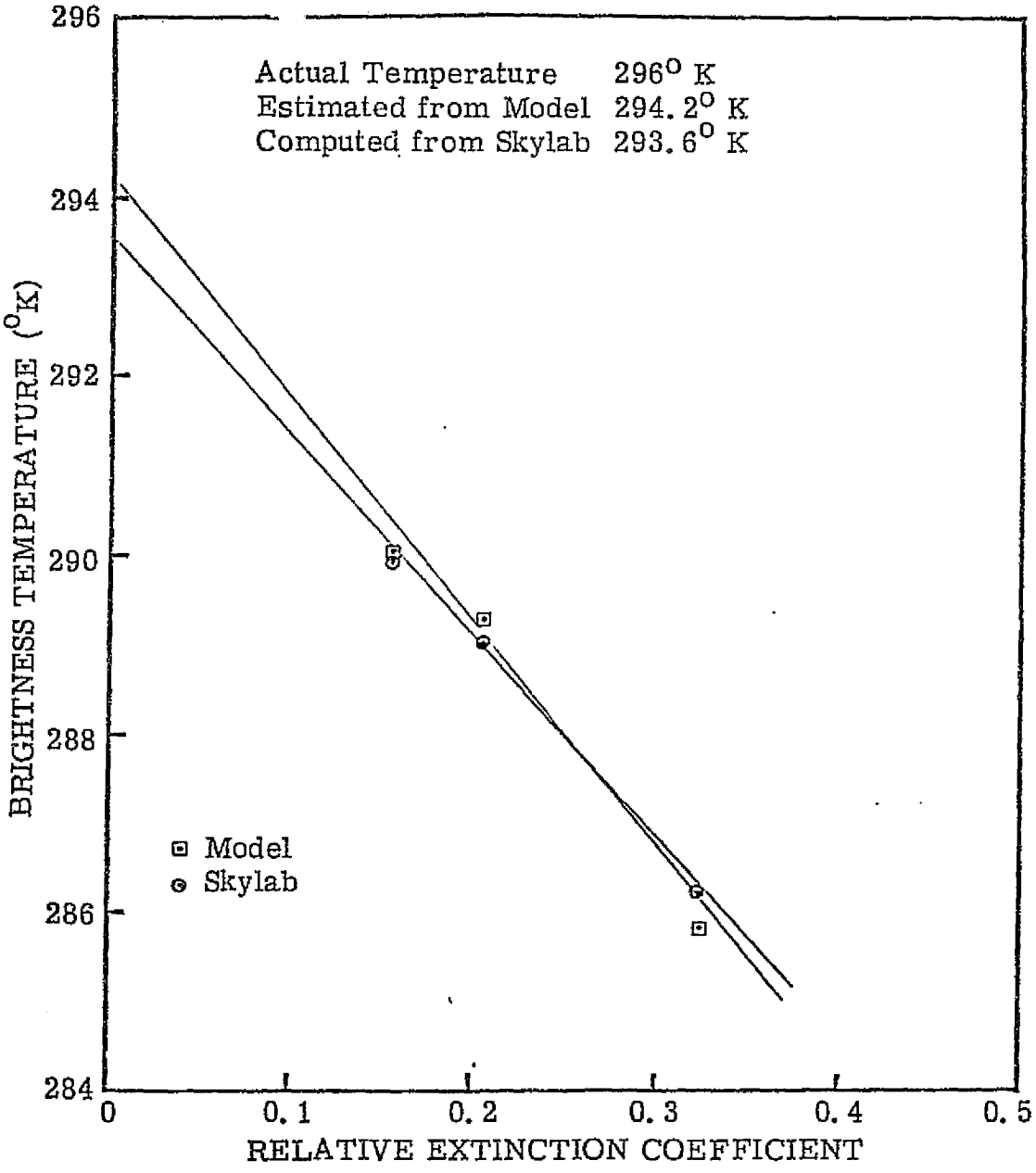

Figure 15. Brightness Temperature Versus Extinction Coefficient for Key West on 8 January 1974. Model predictions compared to S191 measurement predictions.

At the time of data acquisition both PRT-5 radiometric surface temperatures and radiosonde temperature and humidity values were measured. The measured surface temperature was constant at 298^{o}K, except in the shallows which was distant from where the S191 was looking. The radiosonde data are given in Table 3. These data were used as input to the radiative transfer model and the radiance at the S191 aperture was calculated. Also included in the calculation was a 23 km sea level visibility maritime-continental haze. As for Key West haze the extinction coefficients were taken from the work of Fenn [17]. A comparison of calculated and measured radiance is presented in Figure 16. In general the agreement is well within measurement error. Minor differences are noted between 8 and 9 μm, probably caused by the reduced values of aperture brightness temperature. Of major concern to the present study is the spectral region between approximately 10.5 and 13.0 μm, where the agreement is within a few percent. The minor difference at the long wavelength side of the 9.6 μm ozone band is again caused by a lower instrument spectral resolution. It would appear from this comparison that the radiative transfer model is a reasonable representation of reality.

The application of the SST estimation technique to these data was done exactly as for the Key West data. The result is given in Figure 17. Observe that both the model calculations and the EREP data yield an estimate of SST within $\pm$ 1.0^{o} K of the recorded PRT-5 radiometric surface temperature.

Table 3.

Radiosonde Data for Monroe Reservoir,
Salem, Illinois, 10 June 1973

Altitude (meters)	Pressure (mb)	Temperature (^{o}K)	Dew Point Temperature (^{o}K)
0.000	9.980+02	292.36	290.96
8.756+01	9.880+02	296.96	291.96
2.581+02	9.690+02	298.16	290.16
1.154+03	8.740+02	290.96	283.96
1.392+03	8.500+02	290.36	275.36
1.927+03	7.980+02	287.96	257.96
2.314+03	7.620+02	284.76	264.76
2.425+03	7.520+02	283.96	271.96
3.019+03	7.000+02	281.56	251.56
3.752+03	6.400+02	276.76	257.76
4.009+03	6.200+02	276.56	246.56
4.713+03	5.680+02	272.86	242.86
6.310+03	4.630+02	260.86	230.86
9.462+03	3.000+02	235.86	205.86
1.155+04	2.190+02	218.66	.00
1.299+04	1.740+02	207.86	.00
1.343+04	1.620+02	207.66	.00
1.585+04	1.090+02	210.46	.00

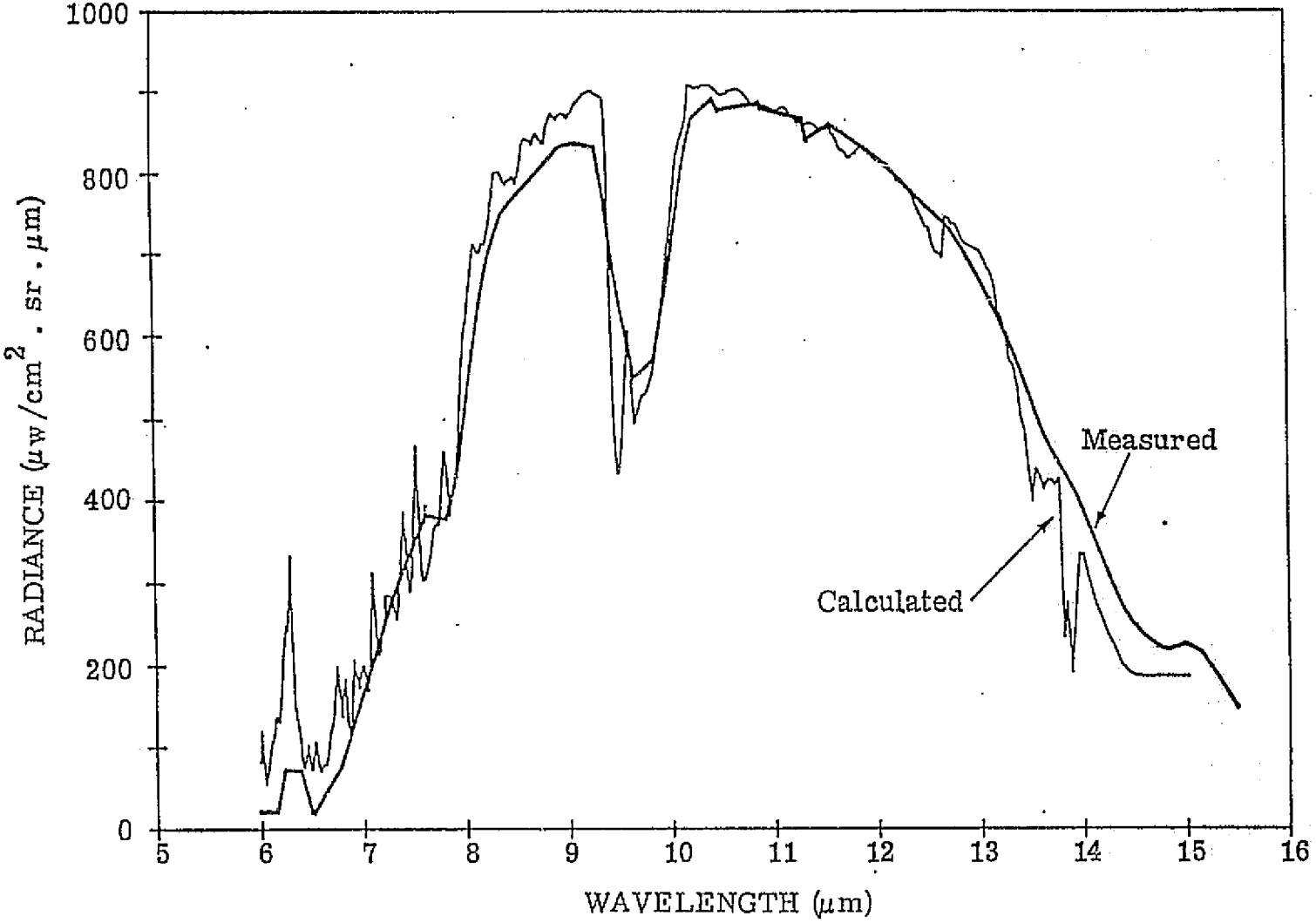

Figure 16. Comparison of Measured and Calculated Spectral Radiance for Monroe Reservoir, Salem, Illinois, on 10 June 1973. SST = 298^{O} K, ϵ = 0.99.

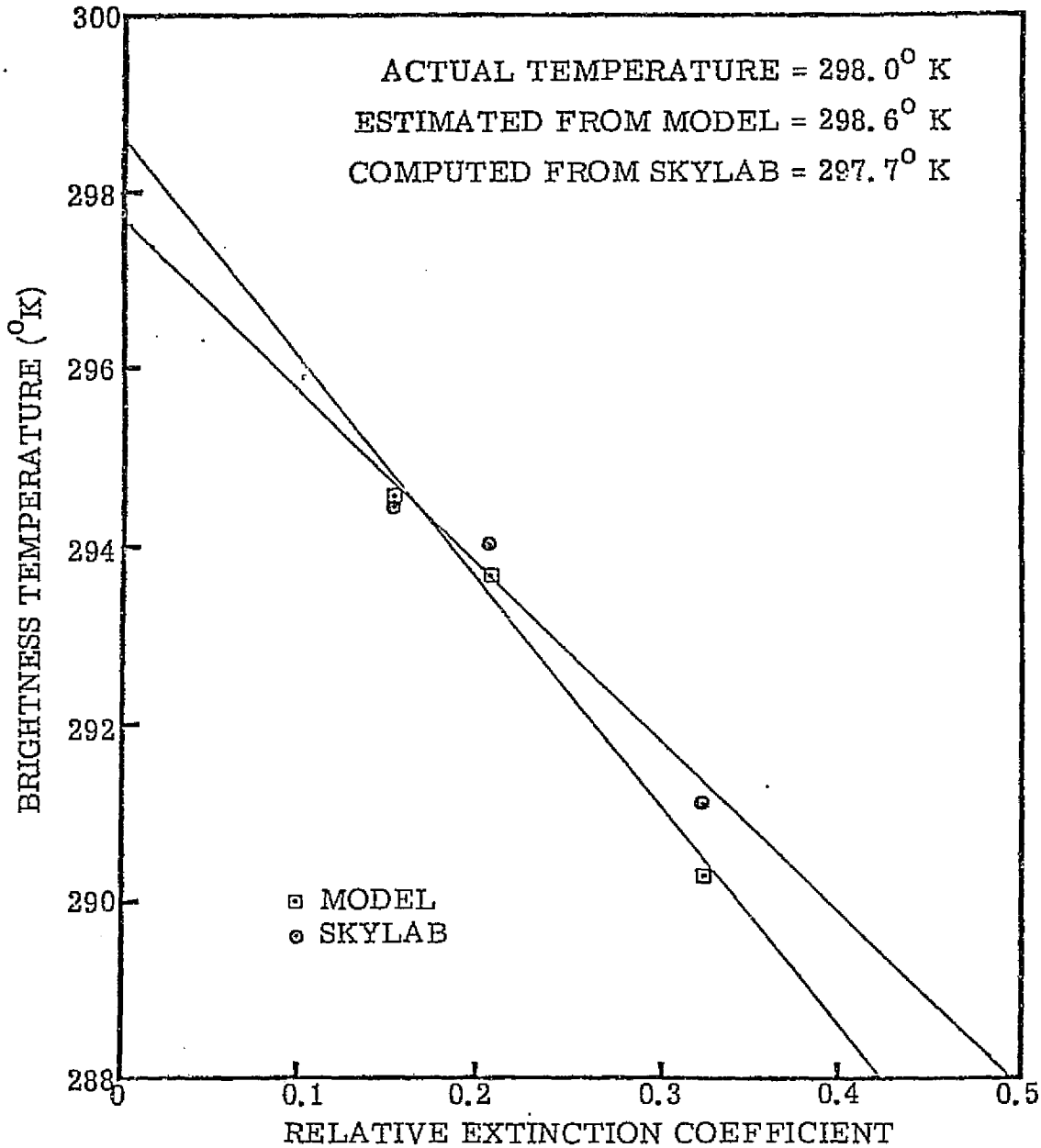

Figure 17. Brightness Temperature Versus Extinction Coefficient for Monroe Reservoir on 10 June 1973. Model Predictions Compared to S191 Measurement Predictions.

5

CONCLUSIONS AND RECOMMENDATIONS

The results presented herein indicate that for purposes of estimating SST from space-acquired data, a significant benefit will be derived by the addition of a second channel in the infrared window region. Specifically, atmospheric-effect uncertainties can probably be reduced to less than 1.0° K without recourse to climatological data. The technique is likely to produce a significant benefit for unusual conditions, such as warm, moist atmospheres over cool waters, or vice versa, when climatological data would yield a particularly poor result.

The present study was of limited scope, with recourse to a limited amount of usable data. Although the study results are indicative, it would be desirable to apply the technique to a broader data base before a final choice is made for the spectral bands to be used in the latter satellites of the TIROS-N series. S191 data could provide that data base if the calibration problems could be overcome and the data corrected. A particularly good set of test sites that could be used for this purpose are those intended for comparative calibration and performance evaluation measurements for the EREP Sensors. These test sites include: The Geysers, California; Rio Grande Reservoir, Colorado; Laguna Reservoir, Arizona; Walker Lake, Nevada; Great Salt Lake, Utah; Dillon Reservoir, Colorado; and Lake Mead, Nevada. The support data for these test sites include the required values of surface temperature and atmospheric meteorology.

REFERENCES

1. W. L. Smith, P. K. Rao, R. Koffer and W. R. Curtis, "The Determination of Sea-Surface Temperature from Satellite High Resolution Infrared Window Radiation Measurements," Monthly Weather Review, Vol. 98, No. 8, Aug. 1970, pp. 604-611.

2. D. Anding and R. Kauth, "Estimation of Sea-Surface Temperature from Space," Remote Sensing of Environment, Vol. 1, 1970, pp. 217-220.

3. L. McMillin, A Method of Determining Surface Temperature from Measurements of Spectral Radiance at Two Wavelengths, Ph. D. dissertation, Iowa State University, 1971.

4. C. Prabhakara, B. Conrath and V. Kunde, Estimation of Sea-Surface Temperature from Remote Measurements in the 11 - 13 μm Window Region, Goddard Space Flight Center, Greenbelt, MD, 1972.

5. J. Price, Analysis of Some Methods for Obtaining Sea-Surface Temperatures from Satellite Observations, Goddard Space Flight Center, Greenbelt, MD, 1973.

6. D. Anding and J. Walker, Use of Skylab EREP Data in a Sea Surface Temperature Experiment, Science Applications, Incorporated, Ann Arbor, MI, First Quarterly Report, JRB-73-202-AA, May 1973.

7. D. Anding and J. Walker, Use of Skylab EREP Data in a Sea Surface Temperature Experiment, Science Applications, Incorporated, Ann Arbor, MI, Fourth Quarterly Report, JRB-74-201-AA, Feb. 1974.

8. D. Anding and J. Walker, Use of Skylab EREP Data in a Sea Surface Temperature Experiment, Science Applications, Incorporated, Ann Arbor, MI, Quarterly Report, JRB-74-202-AA, Sept. 1974.

9. D. Anding and J. Walker, Use of Skylab EREP Data in a Sea Surface Temperature Experiment, Science Applications, Incorporated, Ann Arbor, MI, Interim Report, JRB-75-201-AA, March 1975.

10. D. Anding, J. Hamilton and J. Rowe, Atmospheric Transmission and Emission Program, The Aerospace Corporation, Los Angeles, CA, June 1973.

11. R. M. Goody, Atmospheric Radiation, I Theoretical Basis, Oxford at the Clarendon Press, 1964.

12. R. McClatchey, AFCRL Atmospheric Absorption Line Parameters Compilation, AFCRL, L. G. Hanscom Field, Bedford, Mass., AFCRL-TR-73-0096, Jan. 1973.

13. K. Bignell, Quar. Jour. Roy. Met. Soc., Vol. 96, 1970, p. 390.

14. D. Burch, Investigation of the Absorption of Infrared Radiation by Atmospheric Gases, Philco-Ford Corporation, Aeronutronic Division, Rept. No. U-4784, Jan. 1970.

15. J. McCoy, D. Rensch and R. Long, Applied Optics, Vol. 8, No. 7, 1969.

16. D. Spiegler and J. Greaves, Development of Four-Dimensional Atmospheric Models (Worldwide), Allied Research Associates, Inc., Concord, Mass., NASA CR-61368, Aug. 1971.

17. R. Fenn, Private Communications, AFCRL, Bedford, Mass., 1975.